Chapter 5

Stochastic Radiative Transfer

Shabanov et al.

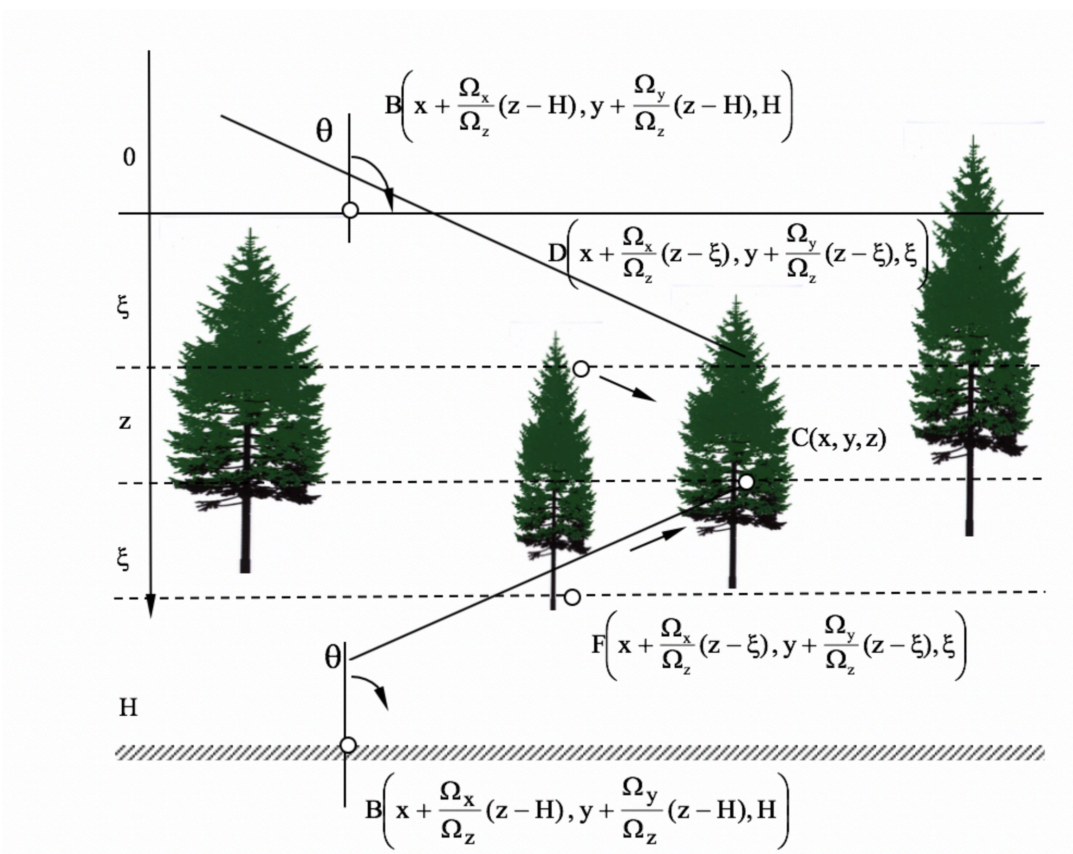

Chapter 5

Stochastic Radiative Transfer

1. Introduction

One key problem of modeling photon transport in vegetation canopies is to account for the three-dimension (3D) canopy structure, which determines the spatial distribution of canopy intercepted solar radiation, or 3D radiation effects [Borel, Gerstl & Powers, 1991; Castel et al., 2001; Jupp et al., 1988, 1989; Knjazikhin et al., 1998a; Li & Strahler, 1992; Myneni & Williams, 1994; Nilson, 1991]. If canopy is short and evenly distributed over the surface (i.e. grass) the *turbid medium* approach is sufficient to represent a canopy structure and the standard 1D Radiative Transfer (RT) equation can be used [Myneni et al., 1997, Ross, 1981]. In contrast, other vegetation biomes, including needle leaf forests, shrublands and savannah, exhibit significant spatial heterogeneity and the full 3D RT modeling is required here [Davis & Knyazikhin, 2005; Myneni, 1991, Myneni et al., 1997]. However, from practical perspective, the use of the 3D RT equation is limited: it requires significant computing resources and, most importantly, numerous input parameters, which are not always available. The approximations are required which are as physically realistic as 3D model and as analytically and operationally compact as 1D model.

Nilson [1991], later Li and Strahler [1992] introduced the *Geometric-Optical* (GO) approach to evaluate radiation reflected by heterogeneous forest stands. The approach utilizes the notion of Bidirectional Gap Probability (probability to observe radiation reflected by vegetation along the direction $\underline{\Omega}$, if it was illuminated by solar radiation along $\underline{\Omega}_0$) and is based on calculation of mutual shadowing by geometrical figures which represent individual trees. The approach provides the physical explanation for the hot-spot effect (the peak in reflected radiation in the retro-illumination direction, due to absence of shadows in this direction). The approach is valid at VIS part of solar spectrum, where one can restrict the study of radiation interaction to that scattered once from the boundary. In the NIR (and larger) wavelengths leaf absorptance is weak, scattering dominates and GO model is not accurate. In order to enable GO model to describe multiple scattering, the original model was enhanced with RT capabilities, resulting in *hybrid Geometric Optical-Radiative Transfer* (GORT) model [Li, Strahler and Woodcock, 1995]. However, combination of models, based on different approaches raised a new problem to preserve energy conservation law.

The alternative to the GO/GORT approach for heterogeneous canopies is to use RT approach in its stochastic formulation. The theory of radiative transfer in stochastic media aims at deriving a closed system of equations which contains the ensemble-average radiation intensity directly as one of its unknown. Specifically, the ensemble of the 3D random realizations of vegetation canopy structure is rendered for a satellite pixel: in each realization, the elementary volume is occupied by vegetation element or gap. The average over ensemble radiation field over pixel corresponds to the mean radiation intensity, measured by remote sensor. The calculation of the average radiation field faces two options. First option is to average canopy physical properties over the ensemble of realizations and substitute them in corresponding 1D RT equation. However, this option is still equivalent to the turbid medium approach. The second option is to average over ensemble the 3D RT equation formulated for particular realization of canopy structure over satellite pixel. This second option is called *stochastic* RT equation. While the averaging procedure results in a 1D RT equation, it is not equivalent to turbid medium case. The stochastic 1D RT equation incorporates 3D radiation effects through correlation of vegetation structure as captured by pair-correlation function.

Radiative transfer in stochastic media has been a highly active research field in recent years [Pomraning, 1991, 1995, 1996; Byrne, 2005]. The first significant attempt to apply stochastic approach to radiative transfer in vegetation was made by Menzhulin and Anisimoiv [1991]. However, the first closed system of stochastic RT equations for mean radiation intensity was derived in application to broken clouds by Vainikko [1973a-b] and further developed by Titov and others [Titov, 1990; Zuev & Titov, 1996; Kasianov, 2003].

In this Chapter we develop the stochastic RT (SRT) approach for discontinuous vegetation canopy by adopting Vainikko equations for broken clouds [1973a-b]. This Chapter is organized as follows. In Section 2 we briefly review 3D RT parameterization. In Section 3 we detail derivation of the SRT equations from 3D RT equation. In Section 4 we develop Boolean model of the air-correlation function, key parameter of the SRT, and discuss its basic properties. Section 5 presents numerical scheme of solution of SRT. The ability of the SRT model to reproduce 3D radiation effects reported in literature is discussed in Section 6. Evaluation of the SRT model with field measurements is presented in Section 7. Finally, Section 8 summarizes key results.

2. 3-D RT Model Parameterization

Consider a discontinuous vegetation canopy of height H in a coordinate system with vertical axis z directed downward (Fig. 1). The spatial structure of such canopy can be characterized by the *indicator function* of canopy, $\chi(\underline{r})$ defined for each elementary volume $d\underline{r}$ at spatial location, $\underline{r}$, as follows:

$$\chi(\underline{r}) = \begin{cases} 1, & \text{if } \underline{r} \in \text{vegetation}, \\ 0, & \text{otherwise.} \end{cases} \tag{1}$$

Density of canopy is defined by the Leaf Area Index (LAI) - one-sided green leaf area per unit ground area [m^2/m^2], namely,

$$\mathrm{LAI} = \frac{1}{S}\int_V dV d_L \chi(\underline{r}) = d_L \int_0^H d\xi \frac{1}{S}\int_s dx dy \chi(x, y, \xi) = d_L \int_0^H d\xi \, p(\xi) \tag{2}$$

where d_L is one-sided foliage area volume density [m^2/m^3], which is assumed to be constant through the space. The integration is performed over a volume of canopy, V, with a footprint, S. The integration of the indicator function over area S results in probability of finding vegetation at particular height ξ (cf. Section 3).

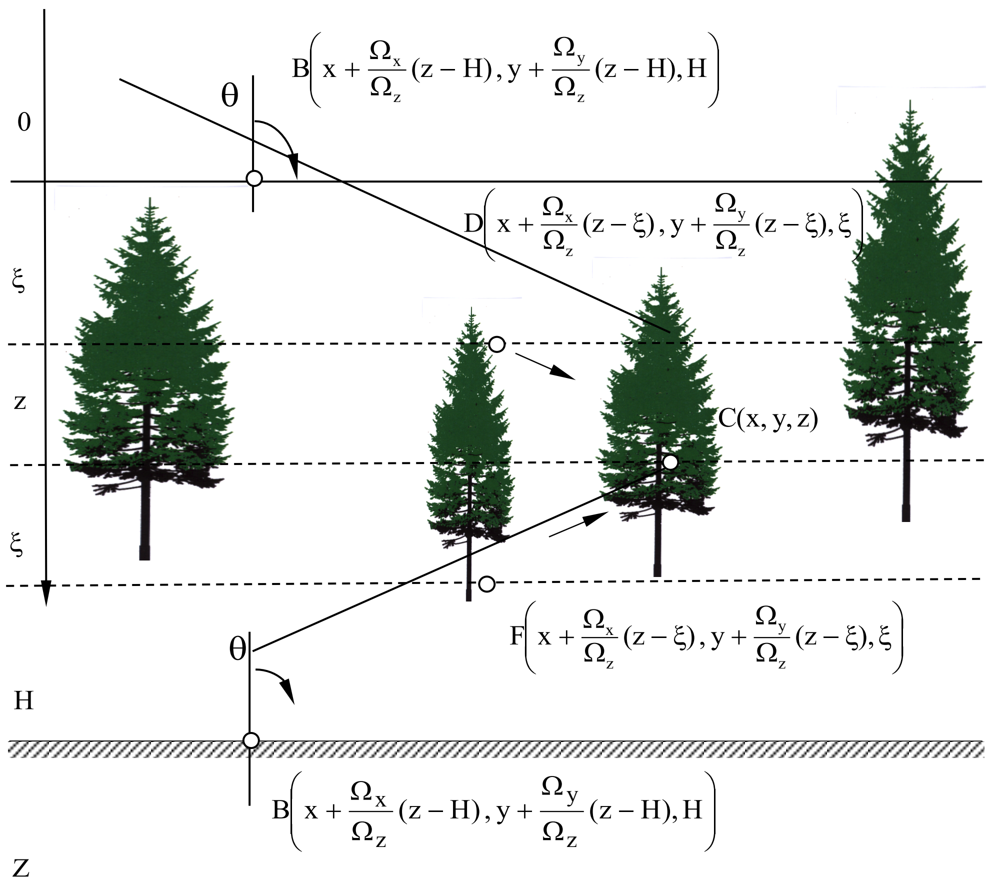

Figure 1. Schematic plot of discontinuous vegetation canopies (needle leaf forests stand) in a coordinate system. The vertical axis, Z, is directed down. Canopy height is H. The angular direction, θ, is measured relative to the upward direction.

The interaction of radiation with canopy leaves is characterized by spatially varying extinction coefficient $\sigma(\underline{r},\underline{\Omega})$ and differential scattering coefficient, $\sigma_S(\underline{r},\underline{\Omega}'\rightarrow\underline{\Omega})$, (Chapter 3),

$$\sigma(\underline{r},\underline{\Omega}) = \sigma(\underline{\Omega})\,\chi(\underline{r}) = d_L\,\chi(\underline{r})\,G(\underline{\Omega}), \tag{3}$$

$$\sigma_S(\underline{r},\underline{\Omega}'\rightarrow\underline{\Omega}) = \sigma_S(\underline{\Omega}'\rightarrow\underline{\Omega})\,\chi(\underline{r}) = \frac{d_L\chi(\underline{r})}{\pi}\Gamma(\underline{\Omega}'\rightarrow\underline{\Omega}), \tag{4}$$

where $G(\underline{\Omega})$ is the mean projection of leaf normals in the direction $\underline{\Omega}$ and $\Gamma(\underline{\Omega}'\rightarrow\underline{\Omega})$ is the area scattering phase function (Chapter 3). The above parameters depend on the probability density of leaf normal orientation, $g_L(\underline{r},\underline{\Omega}_L)$, ($\underline{\Omega}_L$ is a leaf normal direction) and the spectral leaf albedo, $\omega(\underline{r},\lambda)$ (λ is a wavelength). Given the set of structural and optical parameters, the radiation regime in a vegetation canopy is described by the following 3D transport equation for radiation intensity, $I(\underline{r},\underline{\Omega})$:

$$\underline{\Omega}\nabla I(\underline{r},\underline{\Omega}) + \sigma(\underline{r},\underline{\Omega})\,I(\underline{r},\underline{\Omega}) = \int_{4\pi} d\underline{\Omega}'\,\sigma_S(\underline{r},\underline{\Omega}'\rightarrow\underline{\Omega})\,I(\underline{r},\underline{\Omega}'). \tag{5}$$

The unique solution of the Eq. (5) is specified by the following boundary conditions,

$$\begin{cases} I(z=0,\underline{\Omega}) = \dfrac{f_{dir}(\underline{\Omega}_0)}{\left|\mu(\vec{\underline{\Omega}}_0)\right|}\delta(\underline{\Omega}-\underline{\Omega}_0) + (1-f_{dir})d(\underline{\Omega},\underline{\Omega}_0),\ \mu<0, \\ I(z=H,\underline{\Omega}) = \dfrac{\rho_{soil}}{\pi}\displaystyle\int_{2\pi^-} d\underline{\Omega}'\,I(z=H,\underline{\Omega}')\left|\mu(\underline{\Omega}')\right|,\ \mu>0, \end{cases} \tag{6}$$

where the first equation specifies incoming direct, $\delta(\underline{\Omega}-\underline{\Omega}_0)$, and diffuse, $d(\underline{\Omega},\underline{\Omega}_0)$, radiation at the top of canopy, and f_{dir} denotes the ratio of direct to total incoming solar flux. The second equation specifies boundary condition at the canopy bottom, soil surface, which is assumed to be a Lambertian surface with hemispherical reflectance, ρ_{soil}. Note the angular integration notations: integration over the total sphere (4π), lower hemisphere ($2\pi^-$), and upper hemisphere ($2\pi^+$). To simplify numerical solution of the complete RT problem (Eqs. (5) and (6)), two sub-problems with simplified boundary conditions are formulated: 1) the BS-problem: the original illumination condition at the top of the canopy and the soil reflectance is set to 0; 2) the S-problem: there is no input energy from above, but isotropic (Lambertian) sources of energy are uniformly distributed on the canopy bottom. The solution of the complete problem can be approximated by the solutions of the S- and BS- problems as follows,

$$I(\underline{r},\underline{\Omega}) \approx I_{BS}(\underline{r},\underline{\Omega}) + \frac{\rho_{soil}}{1-\rho_{soil}R_S} T_{BS}\, I_S(\underline{r},\underline{\Omega}), \tag{7a}$$

$$R \approx R_{BS} + \frac{\rho_{soil}}{1-\rho_{soil}R_S} T_{BS}T_S, \tag{7b}$$

$$A \approx A_{BS} + \frac{\rho_{soil}}{1-\rho_{soil}R_S} T_{BS}A_S, \tag{7c}$$

$$T \approx T_{BS} + \frac{\rho_{soil}}{1-\rho_{soil}R_S} T_{BS}R_S. \tag{7d}$$

In the equations above, I, I_{BS}, I_S denote radiation intensities, R, R_{BS}, R_S are canopy albedos, A, A_{BS}, A_S are canopy absorptances, T, T_{BS}, T_S are canopy transmittances for the complete, BS- and S- problems, respectively. The above quantities comply with the energy conservation law,

$$R + A + (1-\rho_{soil})T = 1, \tag{8a}$$

$$R_k + A_k + T_k = 1, \tag{8b}$$

where Eq. (8a) refers to the total problem and Eq. (8b) to two sub-problems (k=S or BS).

3. The Stochastic RT Equations

Vegetation canopy as a stochastic medium: We adopt a stochastic view of the landscape and its spatial structure proposed by Jupp et al. [1998]. We describe the 3D canopy structure with the indicator function $\chi(\underline{r})$ (Eq. (1)). Since the vegetation canopy is treated as a stochastic medium, the indicator function is a stochastic function of space. It provides the most general description of the canopy structure that accounts for both its *macroscale* (e.g., dimensions of trees and their spatial distribution) and *microscale* (e.g., the clumping of leaves into tree crown) properties.

Given a realization of the canopy structure, $\chi(\underline{r})$, the corresponding realization of the canopy radiation field is described by the deterministic 3D transport equation (Eqs. (5)-(6)). The averaging of this 3D equation over horizontal plane (cf. next sub-section) results in 1D stochastic RT (SRT) equation for mean intensity. The mathematical formulation of the SRT equation requires two types of averages: (1) $U(z,\underline{\Omega})$, *mean intensity over the portion of the horizontal plane at depth z, occupied by vegetation*; (2) $\bar{I}(z,\underline{\Omega})$, *mean intensity over the total space of the horizontal plane* at depth z,

$$U(z,\underline{\Omega}) \equiv \lim_{R\to\infty} \frac{1}{S_R \cap T_z} \iint_{S_R \cap T_z} dxdy\ \chi(x,y,z) I(x,y,z,\underline{\Omega}), \tag{9}$$

$$\bar{I}(z,\underline{\Omega}) \equiv \lim_{R\to\infty} \frac{1}{S_R} \iint_{S_R} dxdy\ I(x,y,z,\underline{\Omega}). \tag{10}$$

In the above, S_R denotes the area of a circle of radius R; T_z denotes the area of the horizontal plane at depth z, occupied by vegetation. Note, that the mathematical expression, infinite limit on R, may be approximated in practice by the size of finite satellite pixel. Thus, the average intensity, $\bar{I}(z,\underline{\Omega})$, corresponds to satellite measurements over pixel.

The averaging procedure (cf. next sub-section) results in the parameterization of the resulting transfer equation in terms of two stochastic moments of a vegetation structure. The first stochastic moment is the *probability*, p, of finding vegetation at canopy depth z,

$$p(z) \equiv \lim_{R\to\infty} \frac{1}{S_R} \iint_{S_R \cap T_z} dxdy \chi(z,x,y) \equiv \lim_{R\to\infty} \frac{S_R \cap T_z}{S_R}. \tag{11}$$

The second moment is the *pair-correlation function*, q, between vegetation at canopy depth z and at depth ξ along the direction $\underline{\Omega}$,

$$q(z,\xi,\underline{\Omega}) \equiv \lim_{R\to\infty} \frac{S_R \cap T_z \cap T_\xi\left[\frac{\Omega_x}{\Omega_z}(z-\xi), \frac{\Omega_y}{\Omega_z}(z-\xi)\right]}{S_R}. \quad (12)$$

In the above, Ω_x, Ω_y, and Ω_z are projections of a unit direction vector, $\underline{\Omega}$, on the x, y, and z axes, respectively; argument for T_ξ denotes a shift of the origin of plane ξ relative to plane z along x and y directions, required to evaluate correlation between the planes in direction $\underline{\Omega}$ (Fig. 1). In essence, pair-correlation function can be evaluated by taking cross-sections of canopy at depth z and ξ, collapsing cross-sections along direction $\underline{\Omega}$ and measuring the portion of area where both cross-sections indicate vegetation. Using the first and second moments of a vegetation structure, the *conditional pair-correlation* of vegetation structure, K, can be evaluated as

$$K(z,\xi,\underline{\Omega}) \equiv \frac{q(z,\xi,\underline{\Omega})}{p(z)}. \quad (13)$$

Derivation of the Stochastic RT Equations: We follow the procedure of Vainikko [1973a] to derive SRT equations. We start by integrating the 3D RT equation (Eq. 5) from the upper (lower) boundary to some internal point $\underline{r}(z,y,z)$ along the direction $\underline{\Omega}$ (cf. Fig. 1). The resulting equation is,

$$\begin{cases} I(x,y,z,\underline{\Omega}) + \frac{1}{|\mu(\underline{\Omega})|}\int_0^z d\xi\ \sigma(...,\underline{\Omega})I(...,\underline{\Omega}) \\ = \frac{1}{|\mu(\underline{\Omega})|}\int_0^z d\xi \int_{4\pi} d\underline{\Omega}'\ \sigma_S(...,\underline{\Omega}'\to\underline{\Omega})I(...,\underline{\Omega}') + I(x,y,0,\underline{\Omega}), \quad \mu<0, \\ I(x,y,z,\underline{\Omega}) + \frac{1}{|\mu(\underline{\Omega})|}\int_z^H d\xi\ \sigma(...,\underline{\Omega})I(...,\underline{\Omega}) \\ = \frac{1}{|\mu(\underline{\Omega})|}\int_z^H d\xi \int_{4\pi} d\underline{\Omega}'\ \sigma_S(...,\underline{\Omega}'\to\underline{\Omega})I(...,\underline{\Omega}') + I(x,y,H,\underline{\Omega}), \quad \mu>0, \end{cases} \quad (14)$$

where the following short-cut notation was used:

$$(\ldots) = \left(x + \frac{\Omega_x}{\Omega_z}(z-\xi),\ y + \frac{\Omega_y}{\Omega_z}(z-\xi),\ \xi \right). \tag{15}$$

At the next step, Eq. (14) is averaged over the total space of the horizontal plane z. The key problem at this step is to evaluate the integral terms, which involve $\sigma(\ldots,\underline{\Omega})I(\ldots,\underline{\Omega})$ and $\sigma_S(\ldots,\underline{\Omega}' \to \underline{\Omega})I(\ldots,\underline{\Omega}')$. Due to presence of the indicator function in the definition of σ and σ_S (cf. Eqs. (3-4)) the above integrals over the total space of the horizontal plane ξ are reduced to the integrals over the portion of the plane ξ, occupied by vegetation, T_ξ. The integral terms of interest can be evaluated by shifting the origin of T_ξ, in the x-y plane by the vector

$$\left(\frac{\Omega_x}{\Omega_z}(z-\xi), \frac{\Omega_y}{\Omega_z}(z-\xi) \right),$$

followed by integration over vegetation (Eq. (9)):

$$\begin{aligned}
&\frac{1}{S_R}\iint_{S_R} dxdy\ \sigma(\ldots,\underline{\Omega})I(\ldots,\underline{\Omega}) = \\
&= \frac{1}{S_R}\iint_{S_R \cap T_\xi\left[\frac{\Omega_x}{\Omega_z}(z-\xi),\ \frac{\Omega_y}{\Omega_z}(z-\xi)\right]} dxdy\ \sigma(\ldots,\underline{\Omega})I(\ldots,\underline{\Omega}) \\
&= \frac{1}{S_R}\iint_{S_R' \cap T_\xi} dx'dy'\ \sigma(x',y',\xi',\underline{\Omega})I(x',y',\xi',\underline{\Omega}) \\
&= \frac{S_R \cap T_\xi}{S_R} \cdot \frac{1}{S_R \cap T_\xi}\iint_{S_R' \cap T_\xi} dx'dy'\ \sigma(\underline{\Omega})I(x',y',\xi',\underline{\Omega}) \\
&= p(\xi)\sigma(\underline{\Omega})U(\xi,\underline{\Omega})
\end{aligned} \tag{16}$$

Taking into account the derivations above, the equation for mean intensity over total space of horizontal plane at depth z, $\bar{I}(z,\underline{\Omega})$, is

$$
\begin{cases}
\bar{I}(z,\underline{\Omega}) + \dfrac{1}{|\mu(\underline{\Omega})|}\displaystyle\int_0^z d\xi\; p(\xi)\,\sigma(\underline{\Omega})U(\xi,\underline{\Omega}) \\
= \dfrac{1}{|\mu(\underline{\Omega})|}\displaystyle\int_0^z d\xi \int_{4\pi} d\underline{\Omega}'\; p(\xi)\,\sigma_S(\underline{\Omega}' \to \underline{\Omega})U(\xi,\underline{\Omega}') + \bar{I}(0,\underline{\Omega}), \quad \mu < 0, \\
\bar{I}(z,\underline{\Omega}) + \dfrac{1}{|\mu(\underline{\Omega})|}\displaystyle\int_z^H d\xi\; p(\xi)\,\sigma(\underline{\Omega})U(\xi,\underline{\Omega}) \\
= \dfrac{1}{|\mu(\underline{\Omega})|}\displaystyle\int_z^H d\xi \int_{4\pi} d\underline{\Omega}'\; p(\xi)\sigma_S(\underline{\Omega}' \to \underline{\Omega})U(\xi,\underline{\Omega}') + \bar{I}(H,\underline{\Omega}), \quad \mu > 0.
\end{cases}
\tag{17}
$$

In the above, $\bar{I}(0,\underline{\Omega})$ and $\bar{I}(H,\underline{\Omega})$ denote mean radiation intensities over whole horizontal plane at the canopy boundaries; in the typical case of the uniform boundary conditions they are equal to the corresponding 3D values, $I(z=0,\underline{\Omega})$ and $I(z=H,\underline{\Omega})$ (cf. Eq. (6)).

According to Eq. (17), $\bar{I}(z,\underline{\Omega})$, depends on $U(z,\underline{\Omega})$. The equations for $U(z,\underline{\Omega})$ can be derived by averaging Eq. (14) over the portion of a horizontal plane, occupied by vegetation. The terms under the sign of integral in this case can be evaluated with the above described technique (Eq. (16)), taking into account Eqs. (9), (11), and (12), as follows,

$$
\begin{aligned}
&\frac{1}{S_R \cap T_z} \iint_{S_R \cap T_z} dxdy\; \sigma(\ldots,\underline{\Omega})\, I(\ldots,\underline{\Omega}) \\
&= \frac{1}{S_R \cap T_z} \iint_{S_R \cap T_z \cap T_\xi\left[\frac{\Omega_x}{\Omega_z}(z-\xi),\frac{\Omega_y}{\Omega_z}(z-\xi)\right]} dxdy\; \sigma(\ldots,\underline{\Omega})\, I(\ldots,\underline{\Omega}) \\
&= \frac{1}{S_R \cap T_z} \iint_{S'_R \cap T'_z \cap T_\xi} dx'dy'\; \sigma(x',y',\xi',\underline{\Omega}) I(x',y',\xi',\underline{\Omega}) \\
&= \frac{S'_R \cap T'_z \cap T_\xi}{S_R \cap T_z} \frac{1}{S'_R \cap T'_z \cap T_\xi} \iint_{S'_R \cap T'_z \cap T_\zeta} dx'dy'\; \sigma(\underline{\Omega})\, I(x',y',\xi,\underline{\Omega}) \\
&= \frac{q(z,\xi,\underline{\Omega})}{p(z)} \sigma(\underline{\Omega})U(\xi,\underline{\Omega}) \\
&\equiv K(z,\xi,\underline{\Omega})\,\sigma(\underline{\Omega})U(\xi,\underline{\Omega}).
\end{aligned}
\tag{18}
$$

In the above derivations we assumed that the subset $T_z \cap T_\xi$ contains the same percentage of vegetation as the total set T_z. This assumption is similar to one, introduced by Vainikko [1973a] in the derivation of the original version of stochastic equations for atmosphere. This assumption is called "*local chaotisity and global order*" and is required to close system of stochastic equations using only first two moments of structure. Given Eqs. (18) and (14), we can formulate equation for $U(z,\underline{\Omega})$ as follows,

$$\begin{cases} U(z,\underline{\Omega}) + \frac{1}{|\mu(\underline{\Omega})|}\int_0^z d\xi\, K(z,\xi,\underline{\Omega})\,\sigma(\underline{\Omega})U(\xi,\underline{\Omega}) \\ = \frac{1}{|\mu(\underline{\Omega})|}\int_0^z d\xi \int_{4\pi} d\underline{\Omega}'\, K(z,\xi,\underline{\Omega})\,\sigma_S(\underline{\Omega}'\to\underline{\Omega})\,U(\xi,\underline{\Omega}') + U(0,\underline{\Omega}), \quad \mu<0, \\ U(z,\underline{\Omega}) + \frac{1}{|\mu(\underline{\Omega})|}\int_z^H d\xi\, K(z,\xi,\underline{\Omega})\,\sigma(\underline{\Omega})U(\xi,\underline{\Omega}) \\ = \frac{1}{|\mu(\underline{\Omega})|}\int_z^H d\xi \int_{4\pi} d\underline{\Omega}'\, K(z,\xi,\underline{\Omega})\,\sigma_S(\underline{\Omega}'\to\underline{\Omega})U(\xi,\underline{\Omega}') + U(H,\underline{\Omega}), \quad \mu>0. \end{cases} \tag{19}$$

In the above, $U(0,\underline{\Omega})$ and $U(H,\underline{\Omega})$ denote mean radiation intensities over the portion of horizontal plane occupied by vegetation at the canopy boundaries; in the typical case of the uniform boundary conditions they are equal to corresponding 3D values, $I(z=0,\underline{\Omega})$ and $I(z=H,\underline{\Omega})$ (cf. Eq. (6)).

Radiation over Gaps: The complementary variable, mean radiation intensity over gaps, $V(z,\underline{\Omega})$, is not a part of the closed system of stochastic equations (Eqs. (17) and (19)), but it could be useful in applications. It is defined as follows

$$V(z,\underline{\Omega}) \equiv \lim_{R\to\infty}\frac{1}{S_R \cap [S_R - T_z]}\iint_{S_R} dxdy\,[1-\chi(x,y,z)]\,I(x,y,z,\underline{\Omega}), \tag{20}$$

The relationship between $\bar{I}(z,\underline{\Omega})$, $U(z,\underline{\Omega})$ and $V(z,\underline{\Omega})$ is as follows

$$\bar{I}(z,\underline{\Omega}) = \frac{1}{S_R}\iint_{S_R} dxdy\; I(x,y,z,\underline{\Omega})$$

$$= \frac{1}{S_R}\iint_{S_R\cap T_z} dxdy\;\chi(x,y,z)\,I(x,y,z,\underline{\Omega}) + \frac{1}{S_R}\iint_{S_R\cap[S_R-T_z]} dxdy[1-\chi(x,y,z)]\,I(x,y,z,\underline{\Omega})$$

$$= \frac{S_R\cap T_z}{S_R}\,\frac{1}{S_R\cap T_z}\iint_{S_R\cap T_z} dxdy\;\chi(x,y,z)\,I(x,y,z,\underline{\Omega})$$

$$+ \frac{S_R\cap[S_R-T_z]}{S_R}\,\frac{1}{S_R\cap[S_R-T_z]}\iint_{S_R\cap[S_R-T_z]} dxdy\,[1-\chi(x,y,z)]I(x,y,z,\underline{\Omega})$$

$$= p(z)U(z,\underline{\Omega}) - [1-p(z)]V(z,\underline{\Omega}). \tag{21}$$

Separation of Direct and Diffuse Radiation Components: The average intensity over vegetation, $U(z,\underline{\Omega})$, can be decomposed into the direct and diffuse components, according to the pattern of incoming solar radiation, Eq. (6), namely

$$U(z,\underline{\Omega}) = \frac{f_{dir}(\underline{\Omega}_0)}{|\mu(\underline{\Omega}_0)|}U_\delta(z)\delta(\underline{\Omega}-\underline{\Omega}_0) + U_d(z,\underline{\Omega}). \tag{22}$$

Substituting this decomposition into Eq. (19) and collecting terms, which contain the Dirac's delta function, $\delta(\underline{\Omega}-\underline{\Omega}_0)$, we will get equation for the direct component of $U(z,\underline{\Omega})$,

$$U_\delta(z) + \frac{1}{|\mu(\underline{\Omega}_0)|}\int_0^z d\xi\; K(z,\xi,\underline{\Omega}_0)\,\sigma(\underline{\Omega}_0)U_\delta(\xi) = 1, \tag{23}$$

The remaining terms constitute equation for the diffuse component of $U(z,\underline{\Omega})$,

$$\begin{cases} U_d(z,\underline{\Omega}) + \dfrac{1}{|\mu(\underline{\Omega})|}\displaystyle\int_0^z d\xi\ K(z,\xi,\underline{\Omega})\sigma(\underline{\Omega})U_d(\xi,\underline{\Omega}) \\ = \dfrac{1}{|\mu(\underline{\Omega})|}\displaystyle\int_0^z d\xi\ K(z,\xi,\underline{\Omega})S(\xi,\underline{\Omega}) + U_0(z,\underline{\Omega},\underline{\Omega}_0), \quad \mu < 0, \\ U_d(z,\underline{\Omega}) + \dfrac{1}{|\mu(\underline{\Omega})|}\displaystyle\int_z^H d\xi\ K(z,\xi,\underline{\Omega})\sigma(\underline{\Omega})U_d(\xi,\underline{\Omega}) \\ = \dfrac{1}{|\mu(\underline{\Omega})|}\displaystyle\int_z^H d\xi\ K(z,\xi,\underline{\Omega})S(\xi,\underline{\Omega}) + U_H(z,\underline{\Omega},\underline{\Omega}_0), \quad \mu > 0, \end{cases} \tag{24a}$$

where,

$$S(\xi,\underline{\Omega}) = \int_{4\pi} d\underline{\Omega}'\ \sigma_S(\underline{\Omega}' \to \underline{\Omega})U_d(\xi,\underline{\Omega}'), \tag{24b}$$

$$U_0(z,\underline{\Omega},\underline{\Omega}_0) = \frac{f_{dir}(\underline{\Omega}_0)}{|\mu(\underline{\Omega})\mu(\underline{\Omega}_0)|}\int_0^z d\xi\ K(z,\xi,\underline{\Omega})\sigma_S(\underline{\Omega}_0 \to \underline{\Omega})U_\delta(\xi) + [1 - f_{dir}(\underline{\Omega}_0)]d(\underline{\Omega},\underline{\Omega}_0), \tag{24c}$$

$$U_H(z,\underline{\Omega},\underline{\Omega}_0) = \frac{f_{dir}(\underline{\Omega}_0)}{|\mu(\underline{\Omega})\mu(\underline{\Omega}_0)|}\int_z^H d\xi\ K(z,\xi,\underline{\Omega})\sigma_S(\underline{\Omega}_0 \to \underline{\Omega})U_\delta(\xi) + U(H,\underline{\Omega}). \tag{24d}$$

The average intensity over total space of a horizontal plane, $\bar{I}(z,\underline{\Omega})$, can be decomposed similarly to $U(z,\underline{\Omega})$, namely

$$\bar{I}(z,\vec{\Omega}) = \frac{f_{dir}(\underline{\Omega}_0)}{|\mu(\underline{\Omega}_0)|}\bar{I}_\delta(z)\,\delta(\underline{\Omega} - \underline{\Omega}_0) + \bar{I}_d(z,\underline{\Omega}). \tag{25}$$

where $\bar{I}_\delta(z)$ and $\bar{I}_d(z,\underline{\Omega})$ satisfy

$$\bar{I}_\delta(z) = 1 - \frac{1}{|\mu(\underline{\Omega}_0)|}\int_0^z d\xi\ p(\xi)\sigma(\underline{\Omega}_0)U_\delta(\xi), \tag{26}$$

$$\begin{cases} \bar{I}_d(z,\underline{\Omega}) = -\dfrac{1}{|\mu(\underline{\Omega})|}\displaystyle\int_0^z d\xi\ p(\xi)\sigma(\underline{\Omega})U_d(\xi,\underline{\Omega}) \\ +\dfrac{1}{|\mu(\underline{\Omega})|}\displaystyle\int_0^z d\xi\ p(\xi)S(\xi,\underline{\Omega}) + U_0(z,\underline{\Omega},\underline{\Omega}_0), \quad \mu < 0, \\ \bar{I}_d(z,\underline{\Omega}) = -\dfrac{1}{|\mu(\underline{\Omega})|}\displaystyle\int_z^H d\xi\ p(\xi)\sigma(\underline{\Omega})U_d(\xi,\underline{\Omega}) \\ +\dfrac{1}{|\mu(\underline{\Omega})|}\displaystyle\int_z^H d\xi\ p(\xi)S(\xi,\underline{\Omega}) + U_H(z,\underline{\Omega},\underline{\Omega}_0), \quad \mu > 0, \end{cases} \tag{27}$$

and, $S(\xi,\underline{\Omega})$, $U_0(z,\underline{\Omega},\underline{\Omega}_0)$ and $U_H(z,\underline{\Omega},\underline{\Omega}_0)$ are defined by Eq. (24).

Energy Balance: The standard procedure to trace the energy input and output to/from the system is to integrate the equation for the mean intensity [Eq. (17)] over canopy space and over all directions. The resulting canopy reflectance and transmittance are expressed, similar to 1D case, through the mean intensity over total space, $\bar{I}(z,\underline{\Omega})$, as follows

$$R(\lambda) = \int_{2\pi^+} d\underline{\Omega}\,\bar{I}(0,\underline{\Omega})\left|\mu(\underline{\Omega})\right|, \quad T(\lambda) = \int_{2\pi^-} d\underline{\Omega}\,\bar{I}(H,\underline{\Omega})\left|\mu(\underline{\Omega})\right|, \tag{28a}$$

where R and T correspond to reflectance to reflectance and transmittance of the total problem (similar expressions exist for BS and S problem). However, in contrast to canopy reflectance and transmittance, canopy absorptance is expressed through mean intensity over vegetation, $U(z,\underline{\Omega})$. This can be shown as follows,

$$\begin{aligned} A(\lambda) &\equiv \frac{1}{\pi R^2}\int_V d\underline{r}\int_{4\pi} d\underline{\Omega}[1-\omega(\lambda)]\sigma(\underline{\Omega})\,\chi(\underline{r})I(\underline{r},\underline{\Omega}) \\ &= [1-\omega(\lambda)]\int_0^H dz\int_{4\pi} d\underline{\Omega}\,\sigma(\underline{\Omega})\frac{1}{\pi R^2}\int_{\pi R^2} dx\,dy\,\chi(\underline{r})\ I(\underline{r},\underline{\Omega}) \\ &= [1-\omega(\lambda)]\int_0^H dz\int_{4\pi} d\underline{\Omega}\ \sigma(\underline{\Omega})p(z)U(z,\underline{\Omega}). \end{aligned} \tag{28b}$$

Hot-Spot Effect: As of time of writing the major shortcoming of SRT approach is that it does not describe the hot spot effect, just as standard 1D RT equation. While SRT implements the 3D RT effects (cf. Section 5), the reason why it is not describe the hot-spot effect is unknown presently. Thus, the standard approach to implement the hot spot is used, that is to modify the extinction coefficient, $\sigma(\underline{\Omega})$. An important feature of the radiation regime in vegetation canopies is the hot-spot effect, which is the peak in reflected radiance distribution along the retro-illumination direction. The standard theory describes the hot-spot by modifying the extinction coefficient $\sigma(\underline{\Omega})$ namely [Marshak, 1989],

$$\sigma(\underline{\Omega},\underline{\Omega}_0) = \sigma(\underline{\Omega})h(\underline{\Omega},\underline{\Omega}_0),$$

$$h(\underline{\Omega},\underline{\Omega}_0) = \begin{cases} 1-\sqrt{\dfrac{G(\underline{\Omega}_0)\left|\mu(\underline{\Omega})\right|}{G(\underline{\Omega})\left|\mu(\underline{\Omega}_0)\right|}}\exp\left\{-\Delta(\underline{\Omega},\underline{\Omega}_0)k\right\}, & \text{if } (\underline{\Omega}\cdot\underline{\Omega}_0) < 0\,, \\ 1, & \text{if } (\underline{\Omega}\cdot\underline{\Omega}_0) > 0\,, \end{cases}$$

$$\Delta(\underline{\Omega},\underline{\Omega}_0) = \sqrt{\frac{1}{\mu^2(\underline{\Omega}_0)} + \frac{1}{\mu^2(\underline{\Omega})} + \frac{2(\underline{\Omega}\cdot\underline{\Omega}_0)}{\left|\mu(\underline{\Omega})\,\mu(\underline{\Omega}_0)\right|}}. \qquad (29)$$

In the above, k is an empirical parameter, related to the ratio of vegetation height to characteristic leaf dimension, estimated to be between 1 and 8 based [Stewart, 1990].

4. Pair-Correlation Function

Basic Properties of Pair-Correlation Function: In the case of turbid medium three is no correlation between phytoelements and conditional pair-correlation function, K, simplifies:

$$K(z,\xi,\underline{\Omega}) = \frac{q(z,\xi,\underline{\Omega})}{p(z)} \equiv \frac{p(z)\cdot p(\xi)}{p(z)} = p(\xi). \qquad (30)$$

In this case Eq. (17) and (19) are identical. Combining this result with Eq. (21) we have

$$\bar{I}(z,\underline{\Omega}) = U(z,\underline{\Omega}) = V(z,\underline{\Omega}). \qquad (31)$$

Thus, the stochastic equations are reduced to 1D RT equation in the case of turbid medium, where gaps are mixed with vegetation at the level of elementary volume, resulting in lack of distinction between mean intensities over gaps and vegetation. Note that in this case 1D RT equation is formulated with the extinction coefficient $\sigma(z,\underline{\Omega}) = [p(z)\,\mathrm{LAI}]\cdot G(\underline{\Omega})$ and the differential scattering coefficient $\sigma_s(\underline{\Omega}' \to \underline{\Omega}) = [p(z)\,\mathrm{LAI}]\cdot \pi^{-1}\Gamma(\underline{\Omega}' \to \underline{\Omega})$. Thus, solution to the stochastic RT depends on the product $p(z)\,\mathrm{LAI}$ but not on absolute values of $p(z)$ and LAI in this case.

Note the other special property of the pair-correlation function. In the general case of correlation of vegetation structure, the following symmetry property holds true:

$$q(z,\xi,\underline{\Omega}) = q(\xi,z,-\underline{\Omega}). \tag{32}$$

This property directly follows from the definition of the pair-correlation function, Eq. (12).

Boolean Models of Pair-Correlation Function: We follow the theory of *stochastic geometry* [Stoyan, Kendall and Mecke, 1995] to derive analytical expressions for the pair-correlation function in the general case of vegetation structure with correlation. To apply the theory of stochastic geometry to our case we need to reformulate *stochastic 3D model of canopy structure* in terms of *Boolean 2D model of random sets* [Strahler & Jupp, 1990].

Following the concepts of the theory of stochastic geometry, we model the spatial distribution of vegetation species as a stationary *Poisson point process*: a) total number of trees in the bounded study area follows Poisson distribution with intensity (stem density) d; b) spatial distribution of trees is random. We further assume that all trees are identical vertical solids (volume obtained by rotating a curve, r (z), about the vertical axis z).

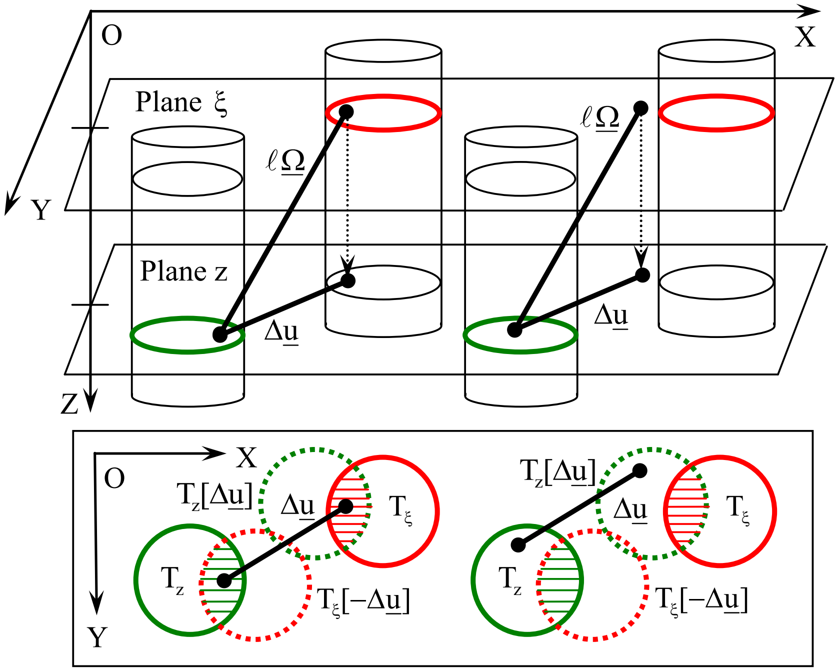

Figure 2. Reducing formulation of pair-correlation function from 3D space (top plot) to 2D Boolean random sets (bottom plot). Cylinders (circles) corresponds to 3D trees (2D projection of trees), while dipole corresponds correlation. If endpoints of 3D dipole, $\ell\underline{\Omega}$, indicate correlation in 3D space, than the 2D projection of dipole, $\Delta\underline{u}$, also indicates correlation (plots at the left) and vice versa (plots at the right).

Now, consider evaluation of the pair-correlation function, $q(z,\xi,\underline{\Omega})$ for the established model of 3D canopy structure (Fig. 2). For simplicity of visualization we represented trees as identical cylinders. Let us define a 3D correlation dipole as a vector $\ell\underline{\Omega}$,

$$\ell\underline{\Omega} \equiv \left(\frac{\Omega_x}{\Omega_z}(z-\xi), \frac{\Omega_y}{\Omega_z}(z-\xi), (z-\xi)\right), \quad \|\ell\underline{\Omega}\| = \ell = \left|\frac{(z-\xi)}{\cos(\underline{\Omega})}\right|, \tag{33a}$$

whose endpoints belong to planes z and ξ. The projection of 3D dipole $\ell\underline{\Omega}$ on a horizontal plane results in a 2D dipole, $\Delta\underline{u}$,

$$\Delta\underline{u} \equiv \left(\frac{\Omega_x}{\Omega_z}(z-\xi), \frac{\Omega_y}{\Omega_z}(z-\xi)\right), \quad \|\Delta\underline{u}\| = \Delta = |(z-\xi)\tan(\Omega)|. \tag{33b}$$

According to definition of $q(z,\xi,\underline{\Omega})$ (Eq. (12)), correlation of vegetation elements between two horizontal planes, z and ξ along the direction $\underline{\Omega}$ in 3D space corresponds to the probability of event when one endpoint of dipole $\ell\underline{\Omega}$ belong to vegetation at plane z (T_z subset), and the other to vegetation at plane ξ (T_ξ subset) ξ (Fig. 2, top portion). To achieve this, the location of one endpoint of dipole is restricted to $T_z \cap T_\xi[-\Delta\underline{u}]$ at the plane z, while the location of the another is simultaneously restricted to $T_z[\Delta\underline{u}] \cap T_\xi$ at the plane ξ. Here argument $\Delta\underline{u}$ corresponds to a shift of subset. Now, we can project 3D stochastic geometry on 2D space, resulting in a union of T_z and T_ξ, $T_z \cup T_\xi$, which is a Boolean random set. Comparing top and bottom portion of Fig. 2, one can see that the location of 3D and 2D dipoles are restricted in the same way to achieve correlation. Comparing such that set of trees will become Boolean random set of trees projection (trees and correlation dipole) on 2D space, one can see that the location of 2D dipole is restricted in the same way as in 3D case. Thus we reduced estimation of pair-correlation function in 3D space to the subject of study stochastic geometry, evaluation of covariance of two points in 2D space of Boolean random sets. Formally,

$$q(z,\xi,\Delta\underline{u}) \equiv \lim_{R\to\infty} \frac{S_R \cap T_z \cap T_\xi[-\Delta\underline{u}]}{S_R} = \Pr[\underline{r}_z,\ \underline{r}_z + \Delta\underline{u} \in T_z \cup T_\xi]. \tag{34}$$

In words, the pair-correlation function is equal to covariance of two points (r_z and $r_z + \Delta\underline{u}$) separated by distance Δ along direction $\underline{u}$ in 2D space of canopy given by union of T_z and T_ξ. In view of azimuthal symmetry of typical landscapes, covariance depends only on absolute value of horizontal distance of correlation, Δ, not direction, $\underline{u}$, that is, $q(z,\xi,\Delta\underline{u}) = q(z,\xi,\Delta)$**.** Below we briefly describe pair-correlation functions for three models Boolean random sets: the Poisson germ-grain, Matérn cluster and Matérn hard-core processes (cf. Fig. 3).

- *Poisson germ-grain model*: In the above formulation of the stochastic model, the points of the Poisson process are germs of the model while the crown cross sections are the primary grains. The primary grains are represented by discs of the radius $r(z)$ and $r(\xi)$. Following derivations of Stoyan, Kendall and Mecke [1995] on p. 68, the covariance function (34) takes the following form

$$q(z,\xi,\Delta) = p(z) + p(\xi) - 1 + [1 - p(z)][1 - p(\xi)]\exp\{d\theta(z,\xi,\Delta)\}, \tag{35a}$$

$$p(z) = 1 - \exp\{-d\pi r^2(z)\}. \tag{35b}$$

Here $p(z)$ is defined by Eq. (11) and, for $r(\xi) \geq r(z)$,

$$\theta(z,\xi,\Delta) = \begin{cases} \pi r^2(z), & \text{if } r(\xi) - r(z) > \Delta, \\ 0, & \text{if } r(\xi) + r(z) \leq \Delta, \\ \alpha r^2(z) + \beta r^2(\xi) - \Delta r(\xi)\sin\alpha, & \text{otherwise,} \end{cases} \tag{35c}$$

$$\alpha = \arccos\left(\frac{r^2(\xi) - r^2(z) + \lambda^2}{2\lambda r(\xi)}\right), \quad \beta = \arccos\left(\frac{r^2(z) - r^2(\xi) + \lambda^2}{2\lambda r(z)}\right). \tag{35d}$$

For $r(\xi) < r(z)$, $\theta(z,\xi,\Delta) = \theta(\xi,z,\Delta)$.

For cylindrical in shape trees, $p(z) = g$, $r(\xi) = r(z) = D_B/2$, $\alpha = \beta = \arccos(\Delta/D_B)$. It follows from Eqs. (35) that the pair correlation function depends on the horizontal distance Δ normalized by the crown base diameter D_B, i.e.,

$$q(\lambda) = 2g - 1 + (1-g)^{2-\kappa(\Delta,D_B)}. \tag{36a}$$

The coefficient $k(\Delta, D_B)$ is an area occupied by the intersection of two circles of the radius D_B shifted by a distance Δ normalized by the circle area $\pi D_B^2/4$, i.e.,

$$k(\Delta, D_B) = 2\pi^{-1}\left[\arccos\frac{\Delta}{D_B} - \frac{\Delta}{D_B}\sqrt{1 - \left(\frac{\Delta}{D_B}\right)^2}\right]\mathcal{H}(D_B - \Delta), \tag{36b}$$

where $\mathcal{H}(s)$ is the Heaviside step function. The derivative at the origin $\lambda = 0$ is

$$\left.\frac{dq(\Delta)}{d\Delta}\right|_{\Delta=0} = \frac{4(1-g)\ln(1-g)}{\pi D_B} . \tag{37}$$

- *Matérn cluster process*: Cluster point processes are derived from the stationary Poisson point process of intensity d by replacing each point with a representative cluster C_0 of points. The representative cluster is a point process. The number of points in C_0 has a Poisson distribution with the positive parameter $\overline{m}$. The points of C_0 are independently and uniformly scattered in the circle of the diameter $D_0 = 2\,r_0$. On each of these points a geometrical figure (clump) is placed. The union of all of these figures is the stochastic cluster model of random sets on the horizontal plane. For clumps represented by circles with the diameter $D_c = 2\,r_c$, the pair-correlation function can be factorized into probabilities of finding two points in the clusters and finding clumps at these points, i.e.,

$$q(\Delta) = \left[2g_c - 1 + (1-g_c)^{2-\kappa(\Delta,D_C)}\right]\left[2g_0 - 1 + (1-g_0)^{2-\kappa(\Delta,D_0)}\right], \tag{38a}$$

$$g_c = 1 - \exp(-\overline{m}\pi\, r_c^2), \quad g_0 = 1 - \exp(-d\pi r_0^2) . \tag{38b}$$

The probability, $p(z)$, of finding a foliated point at depth *z* is given by $p(z) = g_c\, g_0$.

- *Matérn hard-core model*: Tree crowns in the above classes of models may mutually intersect forming complex patterns. The hard-core models describe patterns produced by the locations of centers of non-overlapping circles of a given radius. Consider the Matérn hard-core point process [Stoyan, Kendall & Mecke, 1995] which is derived from a stationary Poisson point process of intensity d by deleting points satisfying some definite rules. Consider a vegetation canopy consisting of cylindrical trees. Let $\eta = \pi D_B^2$, where D_B is the crown base diameter. The intensity,

d_{HC}, and the second order product density, $\rho^2(\Delta)$, of the Matérn hard-core point process are given by [Stoyan, Kendall & Mecke, 1995]

$$d_{HC} = \frac{1-\exp(-d\eta)}{\eta}, \tag{39a}$$

$$\rho^{(2)}(\Delta) = \frac{2\Gamma(\Delta)[1-\exp(-d\eta)] - 2\eta[1-\exp(-d\Gamma(\Delta))]}{\nu\Gamma(\Delta)[\Gamma(\Delta)-\eta]}\mathcal{H}(\Delta - D_B), \tag{39b}$$

$$\Gamma(\Delta) = \eta\left[2 - k(\Delta, 2D_B)\right]. \tag{39c}$$

The second moment $\rho^2(\Delta)$ can be interpreted as the probability density that two tree centers are separated by the distance Δ. Since the trees crowns are assumed to be not overlapping, the ground cover is $g = d_{HC}\pi D_B^2 = d_{HC}\eta/4$. The pair-correlation function is the sum of probabilities of finding foliated points in the same crown and in different crowns, i.e.,

$$q(\Delta) = gk(\Delta, D_B) + \int\limits_{\substack{\|v\|\le D_B \\ \|v'\|\le D_B}} d\underline{v}d\underline{v}'\rho^{(2)}(\|\underline{v} - \underline{v}' + \Delta\underline{u}\|), \tag{39d}$$

where $\underline{u} = (0,1)$ is the unit vector on the plane z=0 and $\|\cdot\|$ is the Euclidean distance. Note the second order product density, $\rho^2(\Delta)$, does not depend on $\underline{u}$.

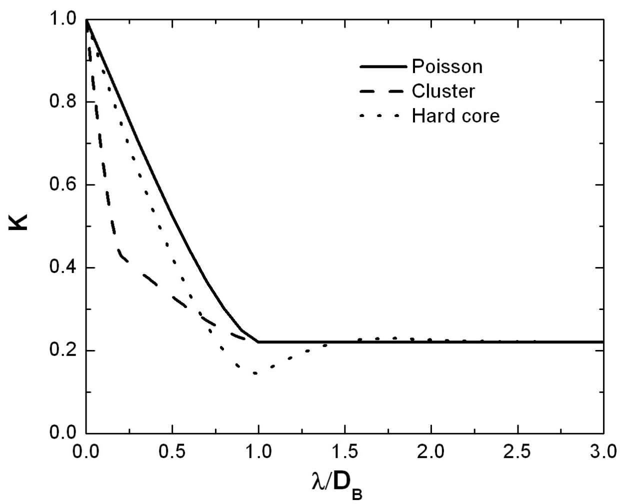

Figure 3. Conditional pair-correlation functions of the Poisson germ-grain, Matérn cluster and Matérn hard-core processes. Cluster, D_0, and clump, D_c, sizes in the Matérn cluster process are set to D_B and $0.2 \cdot D_B$, respectively. The probability, p(z), of finding a foliated point at depth z is 0.22 in all examples.

Pair-Correlation Function and Landscape Properties: It appears that several well known and cdocumented in literature properties of landscape are captured by the pair-correlation function, $q(z,\xi,\Delta)$ or (and) the conditional pair-correlation function, $K(z,\xi,\Delta) \equiv q(z,\xi,\Delta)/p(z)$ (Eqs. (12) and (13)).

First, consider shape of dependence of conditional pair-correlation function, $K(z,\xi,\Delta)$, on correlation distance (cf. Fig. 3). If two points are separated by a short horizontal distance, than $K(z,\xi,\Delta) \to 1$, as $\Delta \to 0$ This property expresses the effect of clumping of foliage elements; that is, detecting a leaf makes it more likely that another leaf will be detected nearby. As correlation distance increases, $K(z,\xi,\Delta)$ reaches its minimum at particular value of distance, which characterizes the crown horizontal size at height z. As horizontal distance increases further, the correlation function tends to increase from its minimum to a constant value, and then levels off. This constant value is the probability, $p(\xi)$, of finding a foliated point at depth ξ (Eq. (30)). Beyond the distance at which correlation function saturates, there is no relation between foliated points.

Second, consider derivative of pair-correlation function, $q(z,\xi,\Delta)$ with respect to correlation distance. Here we rely on the fact that the notion of $q(z,\xi,\Delta)$ is similar to the notion of *semivariance* in the theory of digital image processing, and its spatial derivative at small distances is attributed to the variability of canopy structure at the finest scale [Chen et al., 1993;

Jupp et al., 1989; Roujean, 1999a]. As example, consider $dq/d\Delta$ for $\Delta \rightarrow 0$ for the Poisson germ-grain model of a forest consisting of identical cylindrical trees (Eq. (37)). If the derivative is close to zero (e.g., the horizontal tree dimension D_B is large or the ground cover is close to 1), then vegetation canopy is considered to be a “smooth medium”, whereas if derivative is high, then the canopy structure is “rough.” Inclusion of the within crown leaf spatial correlation will result in a finer scale of the canopy structure variability and value of $|dq/d\Delta|$ at $\Delta \rightarrow 0$ will consequently be higher (curve “Cluster” in Fig. 3).

Finally, it is worth to point to several additional properties of the pair-correlation function, $q(z,\xi,\Delta)$. The extreme case when $\Delta \rightarrow 0$ is realized in two situations: a) when $\xi \rightarrow z$ and b) for vertical directions, when $\theta \rightarrow 0^0\,(180^0)$. In the first case, $q(z,\xi,\Delta) = p(z)$. The second case is more complex. If trees are represented as vertical solids with height dependent radius, r(h) $q(z,\xi,\Delta) = \min\{p(z), p(\xi)\}$. The general case of complex landscape architecture requires calculation according to definition of $q(z,\xi,\Delta)$ (Eq. 12). Nevertheless, under some reasonable simplifying assumptions pair-correlation function conveys information about mean vertical structure when $\Delta \rightarrow 0$. At larger distances, between one and two tree diameter ad depth z, $D(z)$, the pair correlation function provides determines the probability of finding two trees placed Δ apart. In between these extremes, the-pair correlation function describes variation in the canopy structure along different directions, e.g., the distribution of phytoelements that shade leaves at depth ξ along a given direction $\underline{\Omega}$. Overall, the pair-correlation function provides a quantitative description of the canopy structure at all scales of landscape.

5. Numerical Scheme of Solution of the Stochastic RT Equations

According to Eqs. (17) and (19), the solution for the mean intensity over whole horizontal plane, $\bar{I}(z,\underline{\Omega})$, is simply an integration of the mean intensity over vegetation, $U(z,\underline{\Omega})$. Therefore, below we focus on the numerical scheme of solution for the direct and diffuse components of $U(z,\underline{\Omega})$: $U_\delta(z)$ (Eq. (23)) and $U_d(z,\underline{\Omega})$ (Eq. (24)) and. The solution for the direct component requires solution of the parametric Volterra equation. Solution for the diffuse component is based on the Successive Orders of Scattering Approximations (SOSA) iterative method [Myneni et al., 1987]; at each step of iterations we also need to solve the parametric Volterra equations. First, we outline SOSA method in application to stochastic equations. The n-th approximation to the solution for the diffuse component is:

$$U_d^n(z,\underline{\Omega}) = J_1(z,\underline{\Omega}) + J_2(z,\underline{\Omega}) + \ldots + J_n(z,\underline{\Omega}).$$

The functions $J_k(z,\underline{\Omega}), k = 1,2,\ldots,n$ are the solutions of the system of two independent equations (Volterra equations), derived from Eq. (24):

$$J_k(z,\underline{\Omega}) + \frac{\sigma(\underline{\Omega})}{|\mu(\underline{\Omega})|}\int_0^z d\xi\, K(z,\xi,\underline{\Omega})\, J_k(\xi,\underline{\Omega}) = R_{k-1}(z,\underline{\Omega}), \quad \mu < 0, \tag{40a}$$

$$J_k(z,\underline{\Omega}) + \frac{\sigma(\underline{\Omega})}{|\mu(\underline{\Omega})|}\int_z^H d\xi\, K(z,\xi,\underline{\Omega})\, J_k(\xi,\underline{\Omega}) = R_{k-1}(z,\underline{\Omega}), \quad \mu > 0. \tag{40b}$$

The right-hand side of Eq. (40) for n=0 is:

$$R_0(z,\underline{\Omega}) = \frac{f_{dir}(\lambda,\underline{\Omega}_0)\,\sigma_S(\underline{\Omega}_0 \to \underline{\Omega})}{|\mu(\underline{\Omega})\,\mu(\underline{\Omega}_0)|}\int_0^z d\xi\, K(z,\xi,\underline{\Omega}) U_\delta(\xi,\underline{\Omega}) + [1 - f_{dir}(\lambda,\underline{\Omega}_0)] d(\underline{\Omega},\underline{\Omega}_0), \quad \mu < 0,$$

$$R_0(z,\underline{\Omega}) = \frac{f_{dir}(\lambda)\,\sigma_S(\underline{\Omega}_0 \to \underline{\Omega})}{|\mu(\underline{\Omega})\mu(\underline{\Omega}_0)|}\int_z^H d\xi\, K(z,\xi,\underline{\Omega})\, U_\delta(\xi,\underline{\Omega}) + I_H(\underline{\Omega},\underline{\Omega}_0), \quad \mu > 0,$$

If n>0, the right-hand side of Eq (40) is:

$$R_k(z,\underline{\Omega}) = \frac{1}{|\mu(\underline{\Omega})|}\int_0^z d\underline{\Omega} K(z,\xi,\underline{\Omega})\, S_k(\xi,\underline{\Omega}), \quad \mu < 0, \quad \text{when } k \geq 1,$$

$$R_k(z,\underline{\Omega}) = \frac{1}{|\mu(\underline{\Omega})|}\int_z^H d\underline{\Omega}\, K(z,\xi,\underline{\Omega})\, S_k(\xi,\underline{\Omega}), \quad \mu > 0, \quad \text{when } k \geq 1,$$

where the source function $S_k(z,\underline{\Omega})$ is,

$$S_k(z,\underline{\Omega}) = \int_{4\pi} d\Omega' \sigma_S(\underline{\Omega'} \to \underline{\Omega})\, J_k(z,\underline{\Omega'}).$$

The algorithm to solve the system of equations for $U(z,\underline{\Omega})$ is as follows: (1) Find $U_\delta(z,\underline{\Omega})$ from the corresponding Volterra equation [Eq. (23)]; (2) Evaluate $R_0(z,\underline{\Omega})$; (3) Solve the Volterra equations [Eq. (40)] with $R_0(z,\underline{\Omega})$ and find $J_1(z,\underline{\Omega})$; (4) Evaluate $S_1(z,\underline{\Omega}) = = \int_{4\pi} \sigma_S(\underline{\Omega'} \to \underline{\Omega})\, J_1(z,\underline{\Omega'})\, d\underline{\Omega'}$ with $J_1(z,\underline{\Omega})$; (5) Evaluate $R_1(z,\underline{\Omega})$; (6) Calculate $J_2(z,\underline{\Omega})$; (7) Repeat the following until $\left\| J_n(z,\underline{\Omega}) \right\| \le \varepsilon$: (a) Evaluate $S_k(z,\underline{\Omega})$; (b) Calculate $R_k(z,\underline{\Omega})$; (c) Calculate $J_{k+1}(z,\underline{\Omega})$.

The scheme of solution for $U_\delta(z)$ and $U_d(z,\underline{\Omega})$ according to Eqs. (23) and (40) requires the corresponding scheme for the Volterra equation of the following general form:

$$U(z,\underline{\Omega}) + \frac{\sigma(\underline{\Omega})}{|\mu(\underline{\Omega})|} \int_0^z d\xi\, K(z,\xi,\underline{\Omega})\, U(\xi,\underline{\Omega}) = F(z,\underline{\Omega}) \tag{41a}$$

Here $\underline{\Omega}$ is a parameter of the equation. The corresponding discrete scheme is

$$U(k,\underline{\Omega}) + \frac{\sigma(\underline{\Omega})}{|\mu(\underline{\Omega})|} \sum_{j=1}^{j=k} W_{k,j}\, K(k,j,\underline{\Omega})\, U(j,\underline{\Omega}) = F(k,\underline{\Omega}), \tag{41b}$$

where $W_{k,j}$ is the weight, which depends on the numerical scheme used for approximating the integral. Then,

$$U(1,\underline{\Omega}) = F(1,\underline{\Omega}), \text{ when k=1},$$

and when $k \in [2, N_z + 1]$,

$$U(k,\underline{\Omega}) + \frac{\sigma(\underline{\Omega})}{|\mu(\underline{\Omega})|} W_{k,k}\, K(k,k,\underline{\Omega}) U(k,\vec{\Omega}) = F(k,\underline{\Omega}) - \frac{\sigma(\underline{\Omega})}{|\mu(\underline{\Omega})|} \sum_{j=1}^{j=k-1} W_{k,j}\, K(k,j,\underline{\Omega})\; U(j,\underline{\Omega}),$$

$$\Rightarrow \quad U(k,\underline{\Omega}) = \frac{F(k,\underline{\Omega}) - \dfrac{\sigma(\underline{\Omega})}{|\mu(\underline{\Omega})|} \sum\limits_{j=1}^{j=k-1} W_{k,j}\, K(k,j,\underline{\Omega})\, U(j,\underline{\Omega})}{1 + \dfrac{\sigma(\underline{\Omega})}{|\mu(\underline{\Omega})|} W_{k,k}\, K(k,k,\underline{\Omega})}. \tag{42}$$

For angular descretization the ES_n quadratures are optimal to achieve the target accuracy with the minimum amount of nodes [Bass, Voloshenko & Germogenova, 1986; Appendix B]. Generally, about 30 iterations are sufficient to obtain relative accuracy of 10^{-3}. The physical interpretation of the method of successive orders is as follows: the function $J_k(z,\underline{\Omega})$ is the mean intensity of photons scattered k times. The rate of convergence of this method, ρ_c has been defined by Vladimirov [1963], Marchuk and Lebedev [1971] as

$$\| I - I_n \| \le \text{const} \cdot \rho_c{}^n \equiv \text{const} \cdot \big((1 - \exp(-k_0 \cdot H)) \cdot \eta \big)^n, \tag{43a}$$

where k_0 is a certain coefficient and effective single scattering albedo η

$$\eta = \sup_{0<z<H} \sup_{\Omega \in 4\pi} \frac{\sigma_S(\underline{\Omega}_0 \to \underline{\Omega})}{\sigma(z,\underline{\Omega})}. \tag{43b}$$

From Eq. (43) it follows that SOSA converges faster in the case of small optical depth of the layer or in case of small η. If $\eta \approx 1$ and the optical depth is large, the method becomes tedious.

6. Analysis of 3D Radiation Effects

The pair-correlation function naturally arises from averaging the 3D canopy radiation field and, therefore, determines its mean characteristics (Section 3). The aim of this section is to illustrate that the foliage spatial correlation is primary responsible for the 3D effects of the 3D canopy structure on canopy reflective and absorptive properties.

The Poisson germ-grain model of the forest with equal cylindrical in shape trees (Section 4) is used to generate the pair-correlation function simulate the 3D canopy structure. The crown height is H, the crown base diameter is D_B. Non-dimensional scattering centres (leaves) are uniformly distributed and spatially uncorrelated within tree crowns. The probability, p(z), of finding a foliated point at depth *z* (Eq. 11) is constant in this case and coincides with the ground cover *g*, i.e., p(z) = g. The pair-correlation function is given by Eq. (36). The amount of leaf area in the tree crown is parameterized in terms of the plant LAI defined as $L_0 = d_L H$. The canopy LAI is gL_0. Leaf hemispherical reflectance and transmittance are assumed to have the same value and set to 0.07 at Red and 0.38 at the NIR wavelength. Soil reflectance is variable in our calculations. The vegetation canopy is illuminated by a parallel beam of unit intensity. The solar zenith angle set to 30^0.

In addition to simulations in the 3D mode, the stochastic equations were implemented in the 1D mode by utilizing the pair-correlation for turbid medium ($q(z,\xi,\Delta) = p(z) = g = 1$), with other parameters being identical between two modes. Note that in the case when g=1, plant and canopy LAIs coincide (L_0 = LAI). Also, recall that $\bar{I}(z,\underline{\Omega}) = U(z,\underline{\Omega})$ for turbid medium (Eqs. (30)-(31)). The difference in the mean intensities of the 3D and 1D vegetation canopies are utilized to quantify the impact of canopy structure on the canopy radiation regime.

Vertical profiles of radiation fluxes: The upward, $F^{\uparrow}(z)$, and downward, $F^{\downarrow}(z)$, radiation fluxes are derived by integrating mean stochastic intensities over upper and lower hemispheres, that is,

.

$$F_{\Psi}^{\uparrow}(z) \equiv \int_{2\pi^{+}} d\underline{\Omega}\left|\mu(\underline{\Omega})\right|\Psi(z,\underline{\Omega}) \ , \quad F_{\Psi}^{\downarrow}(z) \equiv \int_{2\pi^{-}} d\underline{\Omega}\left|\mu(\underline{\Omega})\right|\Psi(z,\underline{\Omega}), \tag{44}$$

where Ψ stands for $\bar{I}$ (mean intensity over total space), U (mean intensity over vegetation) and

V (mean intensity over gaps). The relationship between $F_I^{\downarrow\uparrow}(z)$, $F_U^{\downarrow\uparrow}(z)$ and $F_V^{\downarrow\uparrow}(z)$ can be established by integrating Eq. (21) over upper and lower hemispheres and substation definitions given by Eq. (44):

$$F_I^{\downarrow\uparrow}(z) - F_U^{\downarrow\uparrow}(z) = (1 - p(z))[F_V^{\downarrow\uparrow}(z) - F_U^{\downarrow\uparrow}(z)]. \tag{45}$$

Note, that in the special case of 1D RT model (turbid medium) there is no distinction between mean intensities over vegetation and gaps (Eq. (30)-(31)), which results in $F_U^{\downarrow\uparrow}(z) = F_V^{\downarrow\uparrow}(z) = F_I^{\downarrow\uparrow}(z) \equiv F_{1D}^{\downarrow\uparrow}(z)$.

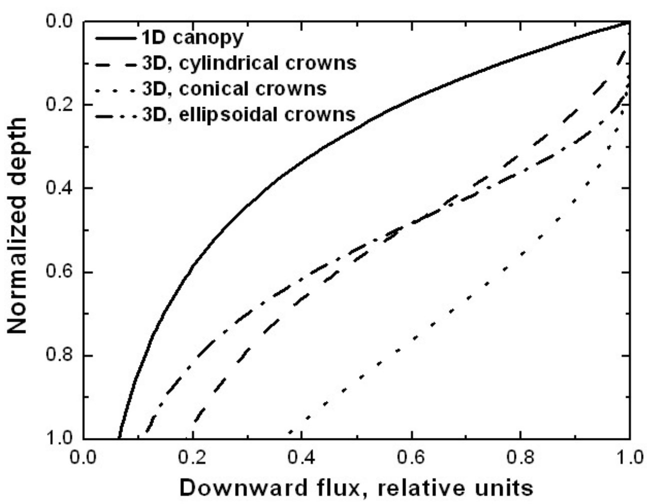

Figure 4. Vertical profiles of mean downward radiation flux densities over between crown space at red wavelength. Calculations are performed for vegetation canopies consisting of cylindrical (dashed line), conical (dotted line) and ellipsoidal (dashed-dotted line) in shape trees. A 1D vegetation canopy is also shown for comparison (solid line). Canopy LAI and ground cover are 4.2 and 0.85, respectively. Soil reflectance is zero.

One key test to verify if RT model capable to simulate 3D radiation effects is to look for the *sigmoidal* shape of the vertical profiles of the between crown downward fluxes, documented by several theoretical and empirical studies [Larsen and Kershaw, 1996; Ni et al., 1997; Roujean, 1999b]. It has been shown that the clumping of phytoelements into tree crown is primarily responsible for this 3D effect [Roujean, 1999b]. Figure 4 shows mean vertical profiles of downward fluxes, averaged over the between crown space, $F_V^{\downarrow}(z)$. Calculations are performed for vegetation canopies consisting of cylindrical, conical and ellipsoidal in shape trees. Equations (35) are used to specify corresponding pair-correlation functions and probabilities, p(z), of finding a foliated point at depth z. In these examples, the ground cover, $g = \max p(z)$, and canopy leaf area index are fixed and equal to 0.85 and 4.2, respectively. Maximum radius of the crown horizontal cross-sections is set to 0.25H where the crown (canopy) height H is 1 (in relative units). One can see that in contrast to 1D model, the stochastic model captures the sigmoidal shape of the vertical profiles of radiations fluxes and the shape is the simulations are sensitive to the crown geometry.

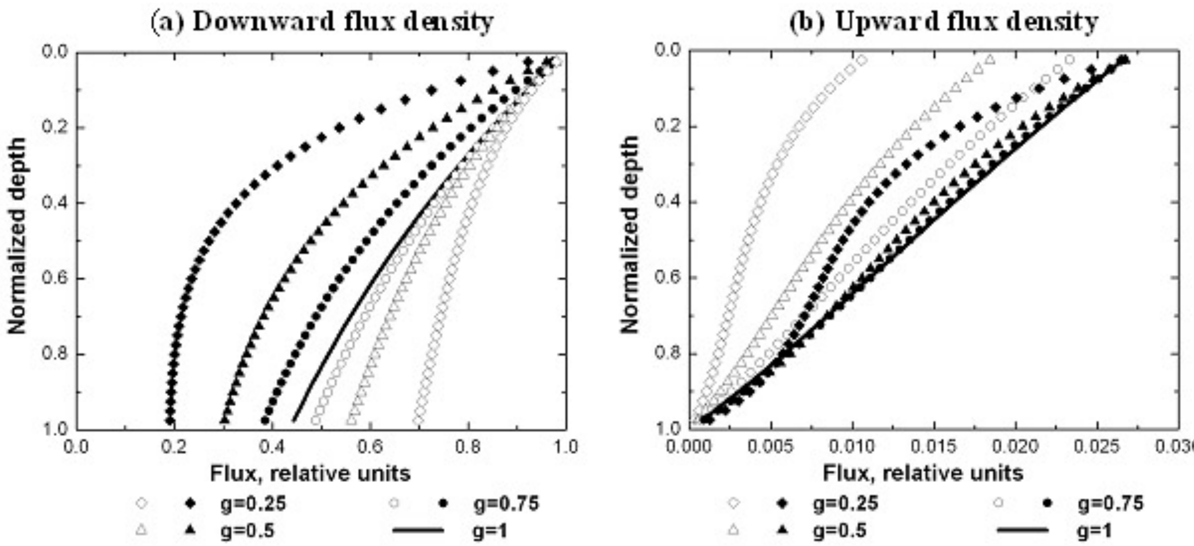

Figure 5. Vertical profiles of mean downward (Panel a) upward (Panel b) radiation flux densities at red wavelength for four values of the ground cover *g*. Ground reflectance is zero. Canopy LAI is fixed and set to 1.5. Plant LAI varies with the ground cover as 1.5/g. The case g=1 (solid lines) corresponds to the 1D vegetation canopy. Solid and hollow symbols represent mean flux densities over crown horizontal cross sections and over the entire horizontal plane, respectively. The dimensionless horizontal axis shows values of z/H_c where H_c is the crown height.

Next, consider vertical profiles of mean downward and upward radiation flux densities accumulated over crown horizontal cross sections ($F_U^{\downarrow}$ and $F_U^{\uparrow}$), and over the total space of horizontal plane ($F_I^{\downarrow}$ and $F_I^{\uparrow}$) as simulated by stochastic model (Fig. 5). For comparison purposes we also present here upward and downward fluxes simulated by 1D model, $F_{1D}^{\downarrow\uparrow}(z)$. First, note that the attenuation of the within crown fluxes is stronger in the case of stochastic model compared to 1D approach, i.e., $F_U^{\downarrow\uparrow}(z) \le F_{1D}^{\downarrow\uparrow}(z)$ (Fig. 5). In this example, LAI=gL_0, a decrease in the ground cover, g, enhances the within crown photon interactions due to an increase in the plant leaf area index L_0 (Fig. 5). Second, note that the tree crowns transmit less radiation compared to horizontally averaged values, i.e., $F_U^{\downarrow}(z) < F_I^{\downarrow}(z)$ (Fig. 5a). It follows from this inequality and Eq. (45) that $F_V^{\downarrow}(z) > F_U^{\downarrow}(z)$ and thus gaps between trees are primarily responsible for the propagation of radiant energy in downward directions. In contrast, upward fluxes have the opposite tendency, i.e., $F_U^{\uparrow}(z) > F_I^{\uparrow}(z)$ (Fig. 5b). For a vegetation canopy bounded from below by a non-reflecting surface, the scattering from leaves determines the upward radiation field. With a fixed amount of the total leaf area, the upward radiation field is an increasing function with respect to the ground cover since an increase in the ground cover involves a decrease in gaps between trees which do not "participate" in the scattering process. Third, note that the reflectance of an individual tree crown, $F_U^{\uparrow}(0)$, is close to the reflectance of the 1D canopy, $F_{1D}^{\uparrow}(0)$. The mean canopy reflectance, $F_I^{\uparrow}(0)$, results from both scattering occurred in tree crowns and "zero scattering" in the between crown space. This lowers the overall canopy reflectance. The 1D approach ignores the gap effect and mean upward radiation flux densities are consequently overestimated.

Energy conservation law: Many ecosystem productivity models and global models of climate, hydrology and ecology need an accurate information on how solar energy is distributed between vegetation canopies and the ground. Using the NCAR Community Climate Model, Buermann et al. [2001] reported that a more realistic partitioning of the incoming solar radiation between the canopy and the underlying ground results in improved model predictions of near-surface climate. The vegetation structure determines the partitioning of the incoming radiation between canopy absorptance, transmittance and reflectance. Here we illustrate the impact of 3D canopy structure on the shortwave energy balance.

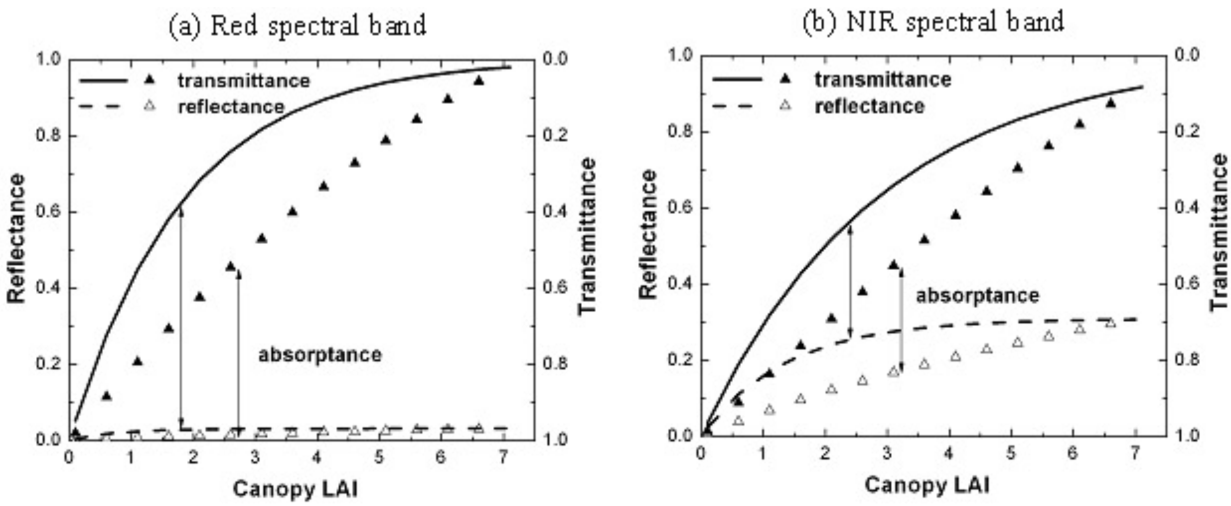

Figure 6. Mean canopy reflectance $F_I^{\uparrow}(0)$ (vertical axis on the left side) and transmittance $F_I^{\downarrow}(1)$ (vertical axis on the right side) at red (Panel a) and near-infrared (Panel b) wavelengths as a function of the canopy LAI. Solid and dashed lines represent the 1D canopy while symbols show its 3D counterpart. Ground reflectance is zero. The canopy absorptance is $1-F_I^{\uparrow}(0)-F_I^{\downarrow}(1)$ (arrows). Plant leaf area index L_0 is fixed and set to 7. Ground cover varies with the canopy LAI as $g = LAI/L_0 = LAI/7$.

Figure 6 shows mean canopy reflectance, $F_I^{\uparrow}(0)$, and transmittance, $F_I^{\downarrow}(1)$. For a vegetation canopy bounded from below by a non reflecting surface, the canopy absorptance is $1 - F_I^{\uparrow}(0) - F_I^{\downarrow}(1)$ as shown in Fig. 8. The 1D approach underestimates canopy transmittance and overestimates canopy reflectance at both Red and NIR wavelengths. As one can see from Fig. 8, these two opposite tendencies do not compensate each other, resulting in an overestimation of canopy absorptance.

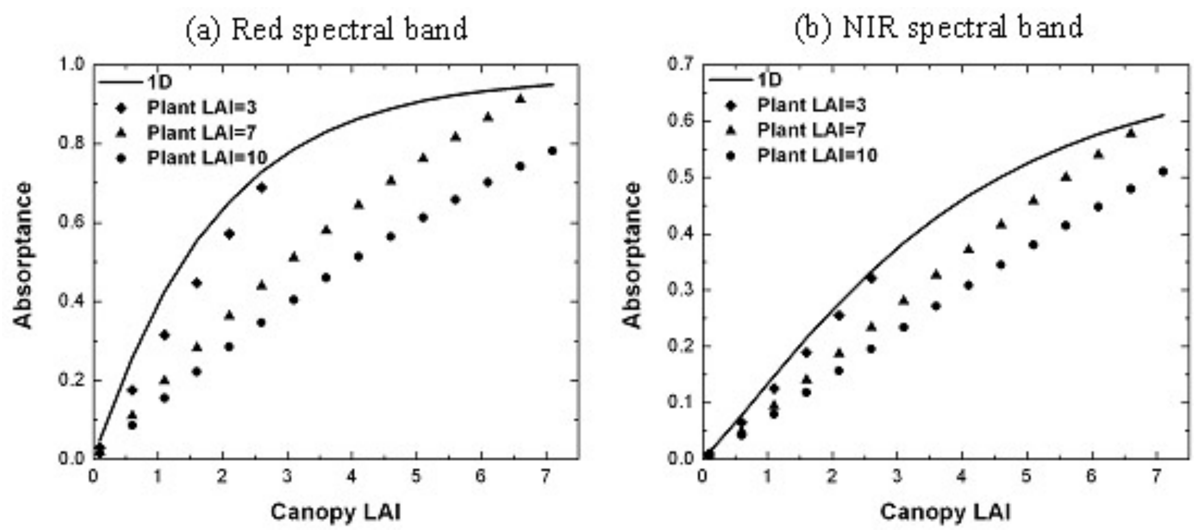

Figure 7. Mean canopy absorptance at red (Panel a) and near infrared (Panel b) wavelengths as a function of canopy LAI for three values of the plant leaf area index L_0. Solid line and symbols represent 1D and 3D vegetation canopies, respectively. Ground cover, g, varies with the canopy LAI as $g = LAI/L_0$. Other parameters are as in Fig. 6

The results given in Fig. 7 show that at a given canopy LAI, canopy absorptance can differ depending upon ground cover and plant LAI. This is not surprising result because a given amount of leaf area can be distributed in different ways in a canopy, for instance, as canopies of dense trees (high plant LAI) with low ground cover or as canopies of sparse trees (low plant LAI) with high ground cover. Although the canopy LAI is the same in both cases, between and within crown radiation regimes are different. Gaps between trees enhance the canopy transmittance at the expense of the canopy absorptance and reflectance. An increase in ground cover involves a decrease in gaps between tree crowns which contribute neither to canopy absorptance nor canopy reflectance. This process enhances canopy reflective (Fig. 6) and absorptive (Fig. 7) properties. It should also be noted that variation in canopy reflectance, absorptance and transmittance with the canopy LAI occurs at a lower rate compared to the 1D model prediction (Figs.6-7). Ignoring the within and between crown radiation regimes can lead to overestimation of the saturation domain, i.e., a range of canopy reflectance values which are insensitive to variation in canopy structure.

Effect of background reflectance: A vegetated surface scatters shortwave radiation into an angular reflectance pattern, or Bidirectional Reflectance Factor (BRF), whose magnitude and shape are governed by the composition, density, optical properties and geometric structure of the vegetation canopy and its underlying surface. By definition, the BRF($\underline{\Omega}$,$\underline{\Omega}_0$) is the surface leaving radiance in direction $\underline{\Omega}$ divided by radiance from a Lambertian reflector illuminated from a single direction, $\underline{\Omega}_0$ [Martonchik et al., 2000]. This parameter has been operationally produced from NASA MODIS and MISR remote sensing measurements [Schaaf et al., 2002; Bothwell at al., 2002].

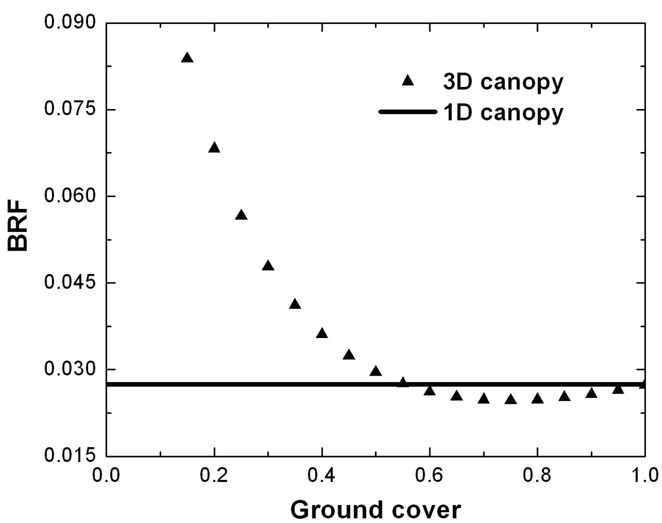

Figure 8. Bidirectional Reflectance Factor (BRF) at red wavelength in nadir view direction as a function of ground cover. Solid line and symbols represent 1D and 3D vegetation canopies, respectively. Canopy LAI is fixed and set to 7. Plant leaf area index varies with ground cover, *g*, as 7/*g*. Surface albedo is 0.18. The solar zenith angle is 30^0. Other parameters are as in Fig. 6.

Figure 8 shows the BRF at red wavelength in the nadir view direction for a vegetation canopy bounded from below by a reflecting surface. For sparse vegetation canopies, photons reflected from the sunlit area of the underlying surface can escape the 3D canopy in the nadir direction without experiencing a collision. This 3D effect results in increased canopy brightness at low ground cover. The BRF exhibits a non monotonic variation with the ground cover. At small-to-moderate values of ground cover, BRF decreases with increasing ground cover due to decrease in the sunlit area which, in turn, reduces the impact of the between crown radiation on the BRF in the nadir direction. However, at sufficiently large ground cover values, the contribution of the underlying surface vanishes and, as in the case of a vegetation canopy with a non–reflecting surface (Figs. 4 and 5b), the BRF becomes an increasing function with respect to the ground cover. As discussed earlier, the 3D effects make BRF values lower compared to those predicted by 1D model. If the leaf spatial correlation is ignored, i.e., $q(z,\xi,\underline{\Omega}) = g^2$, the BRF becomes independent of the ground cover. Thus ignoring the leaf spatial correlation can result in an underestimation of the contribution of canopy background to the canopy leaving radiation for sparse and intermediately dense vegetations and an overestimation of the canopy BRF for dense vegetations. Accounting for 3D effects of underlying vegetation background is especially important in operational algorithms for retrieval of biophysical vegetation biophysical parameters from remote sensing observations over sparse vegetation (savannah, needle leaf forest, etc.)

Canopy structure and NDVI: The measured spectral reflectance data are often transformed into vegetation indices. More than a dozen such indices are reported in the literature and shown to correlate well with vegetation amount [Tucker, 1979], the fraction of absorbed photosynthetically active radiation (FPAR) [Asrar et al., 1984], unstressed vegetation conductance and photosynthetic capacity [Sellers et al., 1992], and seasonal atmospheric carbon dioxide variations [Tucker et al., 1986]. Here we illustrate the impact of 3D canopy structure on relationships between canopy absorption, LAI and the normalized difference vegetation index.

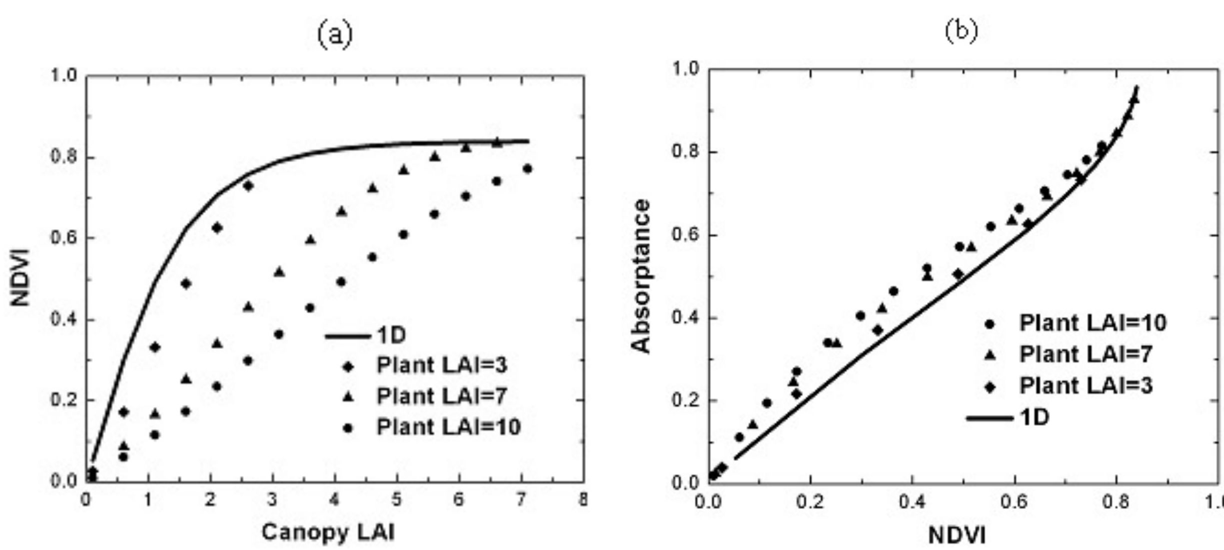

Figure 9. NDVI versus canopy LAI (Panel a) and NDVI versus canopy absorptance (Panel b) canopy absorption at red wavelength for three values of plant leaf area index L_0. Solid line and symbols represent 1D and 3D vegetation canopies, respectively. Ground cover varies with the canopy LAI as $g = LAI/L_0$.

Surface albedo is 0.18 at red and near infrared wavelengths. Other parameters are as in Fig. 7.

The normalized difference vegetation index, NDVI, is defined as the ratio between the difference and the sum of bidirectional reflectance factors at NIR and Red wavelength,

$$\mathrm{NDVI}(\underline{\Omega},\underline{\Omega}_0) = \frac{\mathrm{BRF}_{\mathrm{NIR}}(\underline{\Omega},\underline{\Omega}_0) - \mathrm{BRF}_{\mathrm{RED}}(\underline{\Omega},\underline{\Omega}_0)}{\mathrm{BRF}_{\mathrm{NIR}}(\underline{\Omega},\underline{\Omega}_0) + \mathrm{BRF}_{\mathrm{RED}}(\underline{\Omega},\underline{\Omega}_0)}. \tag{46}$$

This parameter has been operationally produced from NASA MODIS remote sensing measurements [Huete et al., 2002]. Here we consider the NDVI at the nadir view direction.

The relationships between NDVI and canopy LAI are shown in Fig. 9a. The results are similar to those shown in Fig. 7a, i.e., at a given canopy LAI, canopy absorptance and NDVI can differ depending upon ground cover and plant LAI. Different radiation regimes in tree crowns and gaps between them are primarily responsible for this effect. Values of canopy absorptance versus corresponding NDVI values are plotted in Fig. 9b. One can see that the impact of 3D canopy structure on the absorptance-NDVI relationship is minimal. This effect is consistent with the results documented in Asrar et al. [1992], i.e., spatial heterogeneity in vegetation canopies does not affect the relationship between NDVI and fraction of absorbed photosynthetically active radiation (FPAR). The relationship is also insensitive to rather large changes in solar zenith angle [Asrar et al., 1992, Kaufmann et al., 2000]. It should be noted, however, that the NDVI-FPAR relationship is sensitive to the background. Theoretical analyses of these regularities are established in [Myneni et al., 1995; Knyazikhin et al., 1998b; Kaufmann et al., 2000].

7. Model Evaluation with Field Measurements

The internal as well as emergent radiation fields simulated by SRT model were evaluated by comparison to the following sources: (i) RT simulations by 1-D and 3-D RT models [Shultis and Myneni, 1988; Shabanov et al., 2000]; (ii) Monte Carlo simulations of computer generated maize canopy [Espana et al., 1998, Shabanov et al., 2000]; (iii) CIMEL sunphotometer and ground vegetation measurements over shrublands during Jornada PROVE experiment in New Mexico

[Privette et al., 2000, Shabanov et al., 2000]; (iv) SLICER lidar and ground vegetation measurements over several needle leaf forest sites in central Canada and eastern Maryland [Kotchenova et al., 2003]; (v) PARABOLA radiometer and ground vegetation measurements at BOREAS needle leaf forest sites in Canada [Huang et al., 2007]. The last exercise is detailed below.

A field campaign was performed in 1994 as a part of the Boreal Ecosystem-Atmosphere Study (BOREAS) experiment at two sites in the Southern Study Area (SSA), central Saskatchewan, Canada [Deering, Eck & Banerjee, 1999]. The BOREAS designated names for these sites are SSA Old Jack Pine (53.916^{0}N, 104.69^{0}W) and SSA Old Aspen (53.63^{0}N, 106.20^{0}W). A field data set includes forest age, stem density, overstory and understory LAIs [Deering, Eck & Banerjee, 1999], tree height, crown height and horizontal crown radius [Chen, 1996; Hardy et al., 1998], optical properties of leaves, needles and understory [Middleton and Sullivan, 2000; Miller et al., 1997]. The characteristics of each site are summarized in Table 1. Their detailed description can be found in [Deering, Eck & Banerjee, 1999].

Variable	**SSAOJP site**	**SSAOA site**
Stand age, years	68	60
Stem density, stems/ha	2700	1200
LAI	2.2	2.3
Understory LAI	0	3.23
Tree height, m	12.7	16.2
Crown length, m	7	10.76
Horizontal Crown radius, m	1.2	2.12
Leaf/needle reflectance, Red/ NIR	0.100/ 0.62	0.065/ 0.36
Leaf/needle transmittance, Red/ NIR	0.028/ 0.31	0.135/ 0.60
Understory reflectance, Red/ NIR	0.150/ 0.29	0.090/ 0.40

Table 1. Characteristics of the SSA Old Jack Pine (SSAOJP) and SSA Old Aspen (SSAOA) sites used for model parameterization.

The BRF measurements were made with the PARABOLA instrument [Deering and Leone, 1986]. The instrument performs radiance measurements in three narrow spectral bands (650-670 nm, 810-840 nm, and 1620-1690 nm) for almost the complete sky- and ground-looking hemispheres in 15^0 instantaneous field of view [Deering, Eck & Banerjee, 1999]. The instrument was suspended from a tram system mounted at about 13-14m above canopy between two towers spaced about 70 m apart. Total of 11 measurements were taken along the tram at each solar zenith angle. The data were processed to obtain mean BRF over sampling points in 15^0 angular increments in view zenith angle and 30^0 angular increments of view azimuth with one of the bins being centered on the solar principal plane [Deering, Eck & Banerjee, 1999].

The parameters of the SRT model were selected as follows. The Poisson germ-grain model of the forest with identical cylindrical trees (cf. Section 4) was selected to construct the pair-correlation function. The ground cover was estimated with Eq. (35b) where the steam density d and the crown radius $r(z) = D_B/2$ are given in Table 1. Its value is 0.71 for the SSAOJP and 0.82 for the SSAOA site. Given ground cover, the pair-correlation function was calculated using Eq. (36a). The plant leaf area index, L_0=LAI/g, and the leaf area volume density, $d_L=L_0/H_c$ are L_0=3.12, d_L=0.46 for SSAOJP and L_0=2.82, d_L=0.26 for SSAOA. Here H_c and LAI are the crown height and the canopy LAI (Table 1). The optical properties of canopy elementary volume, were calculated based on commonly adopted RT approach, where shoot (not individual needle) represents the basic structural element [Stenberg, 1996; Smolander & Stenberg, 2005]. The measured albedo of individual needles was scaled to shoot level (Table 1) using theory of canopy spectral invariants [Oker-Blom & Smolander, 1988, Smolander & Stenberg, 2005; Chapter 3].

Table 2. Root Mean Square Error in predicting nadir BRF at Red (650-670 nm) and NIR (810-840) spectral bands for SSA Old Jack Pine (SSOJP) and SSA Old Aspen (SSAOA) sites.

	Red spectral band		**NIR spectral band**	
	SSAOJP	**SSAOA**	**SSAOJP**	**SSAOA**
3D canopy	0.0021	0.0013	0.021	0.013
1D canopy	0.0061	0.0024	0.053	0.016

Measured and modeled BRFs at red and NIR wavelengths in the nadir direction as a function of the solar zenith angle for the SSAOJP and SSAOA sites are shown in Fig. 10. The BRFs simulated using the 3D model of canopy structure show very good agreement with measurements (Table 2). If one simplifies the canopy structure into a 1D medium by setting the conditional pair correlation function to its saturated value, ground cover g, the disagreement increases by a factor of about 2.7 for the SSAOJP and 1.5 for SSAOA site (Table 2). In both cases, the 1D approach overestimates the observations. This result is consistent with simulations shown in Fig. 9. The effect of ignoring the leaf spatial correlation is more pronounced at lower ground covers, as expected.

A statistical model given by Eq. (29) was used to simulate the hot spot effect (a sharp peak in reflected radiation about the retro-solar direction). The model requires the specification of a coefficient related to the ratio of vegetation height to the smallest element in the scene. The ratio of tree height to the tree diameter (the finest scale in our simulations) is used. Figure 10 show measured and predicted BRFs and their correlation for the SSAOJP and SSAOA sites. In these examples, the simulations compare well with the field data.

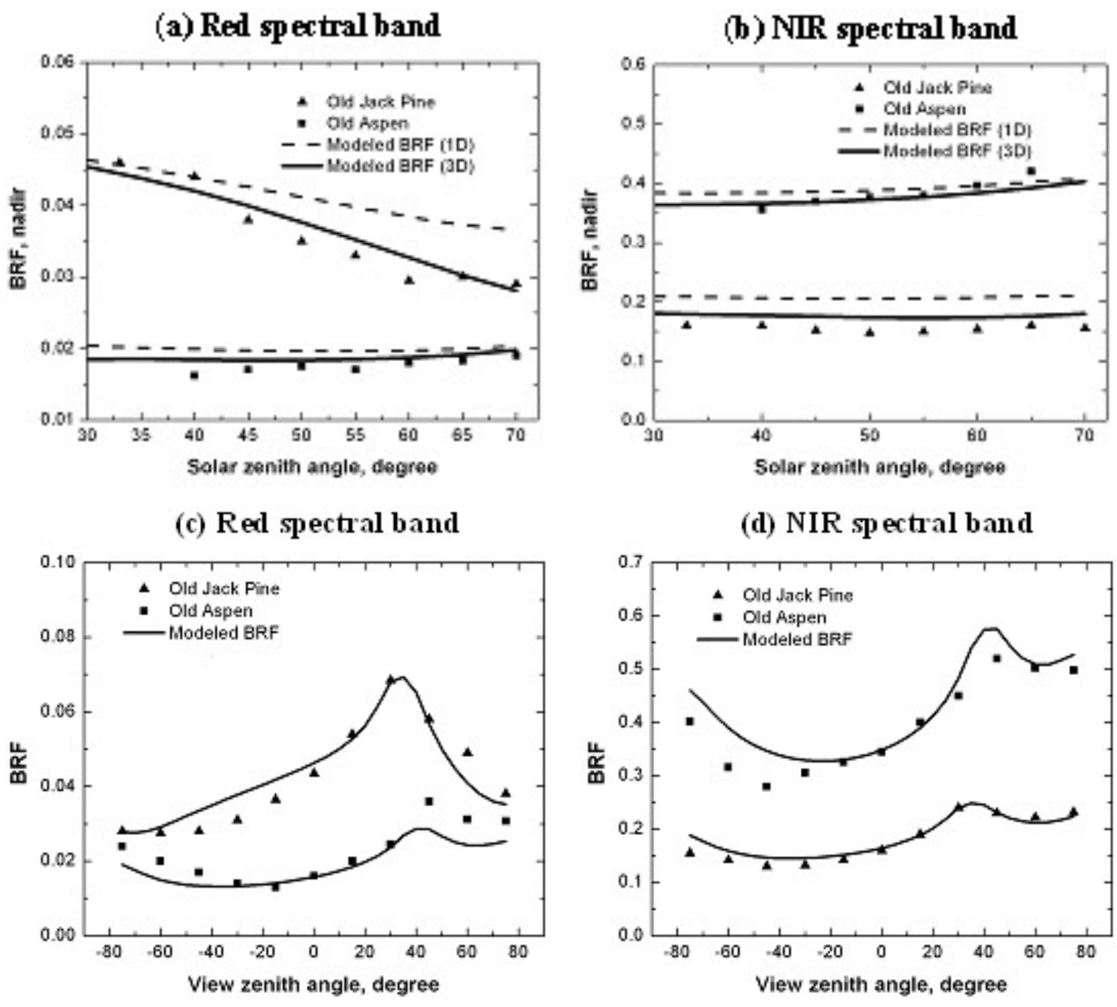

Figure 10. Bidirectional Reflectance Factor at red (Panel a) and NIR (Panel b) wavelengths in the nadir

direction as a function of the solar zenith angle for the SSAOJP and SSAOA sites. Symbols represent measured BRFs. Solid and dashed lines show simulated BRF using 3D and 1D models of canopy structure, respectively. Bidirectional Reflectance Factor in the solar principal plane at red (Panel c) and NIR (Panel d) wavelengths for the SSAOJP and SSAOA sites. The solar zenith angles are 34^0 for SSAOJP and 40^0 for SSAOA. Solid line and symbols represent predicted values and PARABOLA measurements. The RMSE values at red and near infrared spectral bands are 0.0042 and 0.014 for the SSAOJP, 0.0043 and 0.042 for the SSAOA sites.

8. Summary

This chapter introduces the Stochastic Radiative Transfer (SRT) model a powerful RT tool to develop to study biophysical properties of 3D canopy from space measurements. The unique features of the SRT model are: (*i*) its solution coincides exactly with what satellite-borne sensors measure; that is, the mean intensity emanating from the smallest area to be resolved, from a pixel; (*ii*) it accounts for 3D effects through a small set of well defined measurable parameters; and (*iii*) it is as simple as the conventional 1D radiative transfer equation. The 3D canopy structure is accounted in the SRT model with two stochastic moments: (a) probability of finding phytoelements at horizontal plane; and (b) correlation of phytoelements at two horizontal planes. The analysis of the SRT equations indicates that if only the first moment of vegetation structure is used (the case of no correlation), than the SRT model reduces to the 1D turbid medium RT model. Thus, the pair-correlation function is primary responsible for 3D radiation effects. The analytical models of the pair-correlation function, based on theory of Boolean random sets, were in this study. Comparison of 1D and 3D simulations indicates that ignoring the canopy structure can result in an underestimation of the canopy transmittance at the expense of overestimation of the canopy absorptance and reflectance. Transmittance, reflectance and absorptance of the 3D vegetation canopy vary with canopy LAI at a slower rate than 1D model can possible predict. Ignoring this fact in interpretation of satellite data can lead to overestimation of the saturation domain, i.e., a range of canopy reflectance values which are insensitive to variation in canopy structure. The stochastic radiative transfer equations reproduce the effect of sunlit areas of the underlying surface on the canopy leaving radiation. They adequately account for impact of canopy structure on relationships between NDVI, LAI and canopy absorptance. The SRT model was extensively validated with field measurements including comparison with PARABOLA measurements from two coniferous and broadleaf forest stands in BOREAS Southern Study Areas. The performance was found to be satisfactory. At this point, the major shortcoming of the SRT approach is unability to simulate the hot-spot effect, which was implemented in the present version of the SRT model using the standard ad-hook method of modifying the extinction coefficient.

References

Asrar, G., Fuchs, M., Kanemasu, E.T., & Hatfield, J.L. (1984). Estimating absorbed photosynthetic radiation and leaf area index from spectral reflectance in wheat. *Agronomy Journal*, *76*, 300-306.

Asrar, G., Myneni, R.B., & Choudhury, B.J. (1992). Spatial heterogeneity in vegetation canopies and remote sensing of absorbed photosynthetically active radiation: A model study. *Remote Sensing of Environment, 41*, 85–103.

Bass, L., Voloshenko, A.M., and Germogenova, T.A. (1986), *Methods of Discrete Ordinates in Radiation Transport Problems*, Institute of Applied Mathematics, Moscow, pp. 21-23, (in Russian).

Borel, C.C., Gerstl, S.A.W., Powers, B.J. (1991), The radiosity method in optical remote sensing of structured 3-D surfaces. *Remote Sens. Environ*. 36: 13-44.

Bothwell, G.W., Hansen, E.G., Vargo, R.E., & Miller, K.C. (2002). The Multi-angle Imaging SpectroRadiometer science data system, its products, tools, and performance. *IEEE Transactions on Geoscience and Remote Sensing*, *40*, 1467- 1476.

Buermann, W., Dong, J., Zeng, X., Myneni, R. B., & Dickinson, R. E. (2001). Evaluation of the utility of satellite based vegetation leaf area index data for climate simulations. *Journal of Climate 14(17)*, 3536-3550.

Byrne, N. (2005). Three-dimensional radiative transfer in stochastic media. In: A. Marshak and A. B. Davis [Eds.], “*Three Dimensional Radiative Transfer in the Cloudy Atmosphere*,” Springer-Verlag, pp. 385-424.

Castel, T., Beaudoin, A., Floury, N., Le Toan, T., Caraglio, Y., and Barczi, J. F. (2001). Deriving forest canopy parameters for backscatter models using the AMAP architectural plant model. *IEEE Transactions on Geoscience and Remote Sensing*, *39(3)*, 571–583.

Chen, J. M. (1996). Optically-based methods for measuring seasonable variation of leaf area index in boreal conifer stands. *Agricultural and Forest Meteorology*, *80*, 135–163.

Chen, R., Jupp, D.L.B., & Woodcock, C.E. (1993). Nonlinear estimation of scene parameters from digital images using zero-hit run-length statistics. *IEEE Transactions on Geoscience and Remote Sensing*, *31(3)*, 735–746.

Davis, A.B., & Knyazikhin, Y. (2005). A Primer in Three-Dimensional Radiative Transfer. In: A. Marshak and A.B. Davis [Eds.]. "*Three Dimensional Radiative Transfer in the Cloudy Atmosphere*," Springer-Verlag, 153-242.

Deering, D.W., & Leone, P. (1986). A sphere scanning radiometer for rapid directional measurements of sky and ground radiance. *Remote Sensing of Environment*, 19, 1-24.

Deering, D.W., Eck, T. F., & Banerjee, B. (1999). Characterization of the reflectance anisotropy of three boreal forest canopies in spring-summer. *Remote Sensing of Environment*, 67, 205-229.

Espana, M., Baret, F., Chelle, M., Aries, F., Andrieu, B. (1998), A dynamic model of maize 3D architecture: application to the parameterisation of the clumpiness of the canopy. *Agronomie* 18(10): 609-626.

Hardy J.P., R.E. Davis, R. Jordan, W. Ni, & C. Woodcock (1998). Snow ablation modeling in a mature aspen stand of the boreal forest. *Hydrological Processes, 12*, 1763-1778.

Huang, D., Knyazikhin, Y., Wang, W., Deering, W., Stenberg, P., Shabanov., N.V., Tan, B., Myneni, R.B. (2007), Stochastic transport theory for investigating the three-dimensional canopy structure from space measurements. Remote Sensing of Environment, accepted November 2006.

Huete, A., Didan, K., Miura, T., Rodriguez, E.P., Gao, X., and Ferreira, L.G. (2002). Overview of the radiometric and biophysical performance of the MODIS vegetation indices. *Remote Sensing of Environment*, *83*, 195-213.

Jupp, D.L., Strahler, A.H., & Woodcock, C.E. (1988). Autocorrelation and regularization in digital images I. Basic theory. *IEEE Transactions on Geoscience and Remote Sensing*, *26(4)*, 463–473.

Jupp, D.L., Strahler, A.H., & Woodcock, C.E. (1989). Autocorrelation and regularization in digital images II. Simple image models. *IEEE Transactions on Geoscience and Remote Sensing*, *27(3)*, 247–258.

Kasianov E. Stochastic radiative transfer in multilayer broken clouds. Part I: Markovian approach. *Journal of Quantitative Spectroscopy & Radiative Transfer* 2003; 77 (4): 373-393

Kaufmann, R. K., Zhou, L., Knyazikhin, Y., Shabanov, N. V., Myneni, R. B. & Tucker, C. J. (2000). Effect of orbital drift and sensor changes on the time series of AVHRR vegetation index data. *IEEE Transactions on Geoscience and Remote Sensing*, *38(6)*, 2584-2597.

Knyazikhin, Y., Kranigk, J., Myneni, R.B., Panfyorov, O., & Gravenhorst, G. (1998a). Influence of small-scale structure on radiative transfer and photosynthesis in vegetation cover. *Journal of Geophysical Research*, *103*, DD6, 6133-6144.

Knyazikhin, Y., Martonchik, J.V., Diner, D.J., Myneni, R.B., Verstraete, M., Pinty B., Gobron, N. (1998b), Estimation of vegetation canopy leaf area index and fraction of absorbed photosynthetically active radiation from atmosphere-corrected MISR data. *EOS-AM1 special issue of J. Geophys. Res.* 103(D24): 32,239-32,257.

Knyazikhin, Y., Marshak, A., & Myneni, R.B. (2005). Three-Dimensional Radiative Transfer in Vegetation Canopies and Cloud-Vegetation Interaction, In: A. Marshak and A.B. Davis [Eds.]. "*Three Dimensional Radiative Transfer in the Cloudy Atmosphere*," Springer-Verlag, pp. 617-652.

Kotchenova, S.Y., Shabanov, N.V., Knyazikhin, Y., Davis, A.B., Dubayah R., & Myneni, R.B. (2003). Modeling lidar with time-dependent stochastic radiative transfer theory for remote estimation of forest structure. *Journal of Geophysical Research*, 108, Art. No. 4484, 17539-17549.

Larsen, D.R., & Kersaw, Jr., J.A. (1996). Influence of canopy structure assumptions on prediction from Beer's law. A comparision of deterministic and stochastic simulations. *Agricultural and Forest Meteorology*, 81, 61-77.

Li, X, Strahler, A.H. (1992), Geometric-optical bidirectional reflectance modeling of discrete crown vegetation canopy: effect of crown shape and mutual shadowing. *IEEE Trans. Geosci. Remote Sens.* 30(2): 276-292.

Li, X., Strahler, A. H., Woodcock, C.E. (1995), A hybrid Geometric optical-radiative transfer approach for modeling albedo and directional reflectance of discontinuous canopies. *IEEE Trans. Geosci. Remote Sens.* 33(2): 466-480.

Marchuk, G.L., Lebedew, V.I. (1971), *The numerical methods in neutron transport theory*, Atomizdat Publ., Moscow, (in Russian).

Martonchik, J.V., Bruegge, C.J., & Strahler, A. (2000). A review of reflectance nomenclature used in remote sensing. *Remote Sensing Reviews*, *19*, 9-20.

Marshak, A. (1989), Effect of the hot spot on the transport equation in plant canopies. *J. Quant. Spectrosc. Radiat. Transf.* 42: 615-630.

Menzhulin, G. V., Anisimov, O. A., (1991) In *Photon-vegetation interactions. Applications in optical remote sensing and plant ecology* (Myneni, R. B., Ross, J. Ed.), Springer-Verlag, Berlin-Heidelberg., Chap. 4.

Middleton, E., & Sullivan, J. (2000). BOREAS TE-10 Leaf Optical Properties for SSA Species. Data set. Available on-line [http://www.daac.ornl.gov] from Oak Ridge National Laboratory Distributed Active Archive Center, Oak Ridge, Tennessee, U.S.A.

Miller, J. R., White, H. P., Chen, J. M., Peddle, D. R., McDermid, G., Foumier, R. A., Shepherd, P., Rubinstein, I., Freemantle, J., Soffer, R., & LeDrew, E. (1997). Seasonal change in understory reflectance of boreal forests and influence on canopy vegetation indices. *Journal of Geophysical Research*, 102 (D24). 29, 729–736.

Myneni, R.B., Asrar, G. and Kanemasu, E.T. (1987). Light scattering in plant canopies: The method of Successive Orders of Scattering Approximations [SOSA]. *Agric. For. Meteorol*. 39:1-12.

Myneni, R.B. (1991). Modeling radiative transfer and photosynthesis in three-dimensional vegetation canopies. *Agricultural and Forest Meteorology*, 55, 323– 344.

Myneni, R.B., Williams, D.L. (1994). On the Relationship between FAPAR and NDVI. *Remote Sensing of Environment,* 49(3), 200-211.

Myneni, R.B., Hall, F.G., Sellers, P.J., & Marshak, A.L. (1995). The interpretation of spectral vegetation indexes. *IEEE Transactions on Geoscience and Remote Sensing*, *33*, 481-486.

Myneni, R. B., Nemani, R. R., Running S. W. (1997), Estimation of global leaf area index and absorbed PAR using radiative transfer models. *IEEE Trans. Geosci. Remote Sens.* 35(6): 1380-1393.

Ni, W., Li, X., Woodcock, C.E., Roujean, J.L., & Davis, R.E. (1997). Transmission of solar radiation in boreal conifer forests: Measurements and models. *Journal of Geophysical Research*, 102 (D24), 29,555-29,566.

Nilson, T. (1991), In *Photon-vegetation interactions. Applications in optical remote sensing and plant ecology* (Myneni, R. B., Ross, J. Ed.), Springer-Verlag, Berlin-Heidelberg., Chap. 6.

Oker-Blom, P., & Smolander, H. (1988). The ratio of shoot silhouette area to total needle area in Scots pine. *Forest Science 34,* 894-906.

Pomraning, G.C. (1991). *Linear kinetic theory and particle transport in stochastic mixtures*. World Scientific, New Jersey, pp. 235.

Pomraning, G.C., Su, B. (1995), A new higher order closure for stochastic transport equations, proc. *International Conference on Mathematics and Computations, reactor Physics, and Environmental Analyses, American nuclear Society Topical Meeting, Portland, OR*, pp. 537-545

Pomraning, G.C. (1996). Transport theory in discrete stochastic mixtures. *Advances in Nuclear Science and Technology*, *24*, 47–93.

Privette, J.L., Asner, G.P., Conel., J., Nuemmrich, K.F., Olson, R., Rango, A., Rahman, A.F., Thome, K., Walter-Shea, E.A. (2000), The EOS prototype validation excersise (PROVE) at Jornada: Overview and lesson learned. Emote Sensing of Environment, 74(1): 1-12.

Ranson, K. J., Sun, G., Weishampel, J. F., & Knox, R. G. (1997). Forest biomass from combined ecosystem and radar backscatter modeling. *Remote Sensing of Environment*, *59*, 118–133.

Ross, J. (1981). *The Radiation Regime and Architecture of Plant Stands*. Norwell, MA: Dr. W. Junk, pp. 391.

Roujean, J.L. (1999a). Two-Story Equations of Transmission of Solar Energy (TESTSE) in open boreal conifer tree stands. *Journal of Geophysical Research*, 104 (D22), 27,869-27,879.

Roujean, J.L. (1999b). Measurements of PAR transmittance within boreal forest stands during BOREAS. *Agricultural and Forest Meteorology*, *93*, 1-6.

Schaaf, C. B., Gao, F., Strahler, A. H., Lucht, W., Li, X., Tsang, T., Strugnell, N. C., Zhang, X., Jin, Y., Muller, J.-P., Lewis, P., Barnsley, M., Hobson, P., Disney, M., Roberts, G., Dunderdale, M., Doll, C., d'Entremont, R., Hu, B., Liang S., and Privette, J. L. (2002).

First Operational BRDF, Albedo and Nadir Reflectance Products from MODIS. *Remote Sensing of Environment, 83*, 135-148.

Sellers, P.J., Randall, D.A., Betts, A.K., Hall, F.G., Berry, J.A., Collatz, G.J., Denning, A.S., Mooney, H.A., Nobre, C.A., Sato, N., Field, C.B., & Henderson-sellers, A. (1992). Modeling the exchanges of energy, water, and carbon between continents and the atmosphere. *Science*, *275*, 502-509.

Shabanov, N, V., Knyazikhin, Y., Baret, F., & Myneni, R. B. (2000). Stochastic modeling of radiation regime in discontinuous vegetation canopies. *Remote Sensing of Environment*, *74(1)*, 125-144.

Shultis, J.K., Myneni, R.B. (1988), Radiative transfer in vegetation canopies with an isotropic scattering. *J. Quant. Spectrosc. Radiat. Transf.* 39:115-129.

Smolander, S., & Stenberg, P. (2005). Simple parameterizations of the radiation budget of uniform broadleaved and coniferous canopies. *Remote Sensing of Environment, 94*, 355–363.

Stenberg, P. (1996). Simulations of the effect of shoot structure and orientation on vertical gradients in intercepted light by conifer canopies. *Tree Physiology, 16*, 99-108.

Stewart, R. (1990), Modeling radiant energy transfer in vegetation canopies, M.S. Thesis, Kansas State University, Manhattan, Kansas, 66506.

Stoyan, D., Kendall, S. W., & Mecke, J. (1995). *Stochastic Geometry and its Application*. John Wiley & Sons, New York, pp. 436.

Strahler, A.H., & Jupp, D.L.B. (1990). Modeling bidirectional reflectance of forests and woodlands using Boolean models and geometric optics. *Remote Sensing of Enviroment*, *34*, 153–160.

Titov, G.A. (1990). Statistical description of radiation transfer in clouds. *Journal of the Atmospheric Sciences*, *47*, 24–38.

Tucker, C.J. (1979). Red and photographic infrared linear combination for monitoring vegetation. *Remote Sensing of Environment*, *8*, 127-150.

Tucker, C.J., Fung, Y., Keeling, C.D., & Gammon, R.H. (1986). Relationship between atmospheric CO_2 variations and a satellite-derived vegetation index. *Nature*, *319*, 195-199.

Vainikko, G.M. (1973a), The equation of mean radiance in broken cloudiness. *Trudy MGK SSSR, Meteorological investigations* 21: 28-37, (in Russian).

Vainikko, G.M. (1973b), Transfer approach to the mean intensity of radiation in noncontinuous clouds. *Trudy MGK SSSR, Meteorological investigations* 21: 38-57, (in Russian).

Vladimirov, V.S. (1963), *Mathematical problems in the one-velocity theory of particle transport*, Tech. Rep. AECL-1661, At. Energy of can. Ltd., Chalk River, Ontario.

Zuev, V.E., Titov, G.A. (1996), *Atmospheric optics and climate.* The series 'Contemporary problems of atmospheric optics', Vol.9, Spector, Institute of Atm. Optics RAS, (in Russian).